TECHNICAL REPORT STANDARD PAGE

1. Title and Subtitle

Development of a Cyclic Semi-Circular Bend Test to Evaluate Asphalt Mixture Crack Propagation Properties at Intermediate Temperature

2. Author(s)

Louay Mohammad, Ph.D., P.E. (WY), F. ASCE;
Ye Ma, Ph.D.

3. Performing Organization Name and Address

Department of Civil and Environmental Engineering
Louisiana State University
Baton Rouge, LA 70803

4. Sponsoring Agency Name and Address

Louisiana Department of Transportation and Development
P.O. Box 94245
Baton Rouge, LA 70804-9245

5. Report No.

FHWA/LA.25/710

6. Report Date

June 2025

7. Performing Organization Code

LTRC Project Number: 21-1B
SIO Number: DOTLT1000390

8. Type of Report and Period Covered

Final Report
01/2021–06/2024

9. No. of Pages

102

10. Supplementary Notes

Conducted in Cooperation with the U.S. Department of Transportation, Federal Highway Administration.

11. Distribution Statement

Unrestricted. This document is available through the National Technical Information Service, Springfield, VA 21161.

12. Key Words

Asphalt mixture; fatigue cracking; cyclic semi-circular bending; Digital Image Correlation; Paris' Law model.

13. Abstract

The Semi-Circular Bend (SCB) test has traditionally been conducted in a monotonic loading and displacement-controlled mode at intermediate temperatures to assess the fatigue crack resistance of asphalt mixtures. However, fatigue damage is essentially the deterioration of material integrity as a result of repeated loading. The monotonic loading of the SCB does not accurately represent the repetitive nature of traffic loads. This may have limitations on the mechanism of fatigue cracking in asphalt mixtures. This study aims to develop a cyclic SCB test protocol to characterize the fatigue cracking of asphalt mixtures. A secondary goal is to apply the Paris' Law coefficients obtained from the proposed cyclic SCB test in the pavement fatigue model for predicting pavement

fatigue life. Digital Image Correlation (DIC) system configurations were set up for deformation and crack propagation measurements of mixture samples during cyclic SCB testing. Two indicators, including the number of cycles to failure and Paris' Law coefficients, were used to characterize the fatigue cracking resistance of asphalt mixtures. The testing parameters of the cyclic SCB test, including notch depth and load frequency, were optimized, and a sensitivity analysis was designed and conducted for the proposed cyclic SCB test protocol using three asphalt mixtures with differing levels of cracking performance. To address the limitations of previous approaches that relied on indirect estimation and manual labeling during the analysis process, an innovative method was developed to directly measure the crack length during the cyclic SCB test. Additionally, the results of the Paris' Law coefficients determined from the cyclic SCB test were utilized to predict the fatigue life of asphalt pavement.

The results indicated that the Paris' Law coefficients have relatively low variance compared to the number of cycles to failure and are independent of notch depth and loading frequency. The optimal testing parameter combination of 25 mm notch depth and 10 Hz loading frequency was recommended from the perspective of test variance and practicability. The Paris' Law parameter *n* was found to have good agreement with the expected rank of fatigue cracking resistance. The Paris' Law coefficient, determined using an innovative approach, effectively differentiated mixtures with varying fatigue cracking resistance. The Paris' Law fatigue model, which is based on fracture mechanic principles, exhibited greater sensitivity to mixtures with varying cracking performances compared to the classic Pavement ME fatigue model.

Project Review Committee

Each research project will have an advisory committee appointed by the LTRC Director. The Project Review Committee is responsible for assisting the LTRC Administrator or Manager in the development of acceptable research problem statements, requests for proposals, review of research proposals, oversight of approved research projects, and implementation of findings.

LTRC appreciates the dedication of the following Project Review Committee Members in guiding this research study to fruition.

LTRC Administrator/Manager

Samuel B. Cooper III, Ph.D., P.E.
Materials Research Administrator

Members

Luanna Cambas
Xingwei Chen
David Madden
Don Weathers
Jason Davis

Directorate Implementation Sponsor

Chad Winchester, P.E.
DOTD Chief Engineer

Development of a Cyclic Semi-Circular Bend Test to Evaluate Asphalt Mixture Crack Propagation Properties at Intermediate Temperature

By
Louay Mohammad, Ph.D., P.E. (WY), F.ASCE
Ye Ma, Ph.D.

Louisiana Transportation Research Center
4101 Gourrier Avenue
Baton Rouge, LA 70808

LTRC Project No. 21-1B
SIO No. DOTLT1000390

conducted for
Louisiana Department of Transportation and Development
Louisiana Transportation Research Center

June 2025

Abstract

The Semi-Circular Bend (SCB) test has traditionally been conducted in a monotonic loading and displacement-controlled mode at intermediate temperatures to assess the fatigue crack resistance of asphalt mixtures. However, fatigue damage is essentially the deterioration of material integrity as a result of repeated loading. The monotonic loading of the SCB does not accurately represent the repetitive nature of traffic loads. This may have limitations on the mechanism of fatigue cracking in asphalt mixtures. This study aims to develop a cyclic SCB test protocol to characterize the fatigue cracking of asphalt mixtures. A secondary goal is to apply the Paris' Law coefficients obtained from the proposed cyclic SCB test in the pavement fatigue model for predicting pavement fatigue life. Digital Image Correlation (DIC) system configurations were set up for deformation and crack propagation measurements of mixture samples during cyclic SCB testing. Two indicators, including the number of cycles to failure and Paris' Law coefficients, were used to characterize the fatigue cracking resistance of asphalt mixtures. The testing parameters of the cyclic SCB test, including notch depth and load frequency, were optimized, and a sensitivity analysis was designed and conducted for the proposed cyclic SCB test protocol using three asphalt mixtures with differing levels of cracking performance. To address the limitations of previous approaches that relied on indirect estimation and manual labeling during the analysis process, an innovative method was developed to directly measure the crack length during the cyclic SCB test. Additionally, the results of the Paris' Law coefficients determined from the cyclic SCB test were utilized to predict the fatigue life of asphalt pavement.

The results indicated that the Paris' Law coefficients have relatively low variance compared to the number of cycles to failure and are independent of notch depth and loading frequency. The optimal testing parameter combination of 25 mm notch depth and 10 Hz loading frequency was recommended from the perspective of test variance and practicability. The Paris' Law parameter *n* was found to have good agreement with the expected rank of fatigue cracking resistance. The Paris' Law coefficient, determined using an innovative approach, effectively differentiated mixtures with varying fatigue cracking resistance. The Paris' Law fatigue model, which is based on fracture mechanic principles, exhibited greater sensitivity to mixtures with varying cracking performances compared to the classic Pavement ME fatigue model.

Acknowledgements

The research reported in this report was sponsored by the Louisiana Department of Transportation and Development (DOTD) through the Louisiana Transportation Research Center (LTRC). The authors would like to express their thanks to the staff of the Asphalt Research Laboratory and all those who have provided valuable help in this study.

Implementation Statement

It is anticipated that the results from this study will provide guidance to state agencies in the development of a standard test to evaluate the fatigue cracking resistance of asphalt mixtures.

Table of Contents

List of Tables

List of Figures

Introduction

Ensuring adequate crack resistance in asphalt concrete (AC) is critical for asphalt pavement performance. The Louisiana Department of Transportation and Development (DOTD) currently mandates the use of the Semi-Circular Bend (SCB) test as part of its balanced mix design framework for paving asphalt mixtures [1]. The SCB test is conducted at 25°C in accordance with ASTM D8044 to obtain the critical strain energy release rate (J_c), an indicator of the crack resistance of asphalt mixtures. The Louisiana DOTD specification stipulates a minimum J_c of 0.6 kJ/m^2 for Level 2 mixtures and 0.5 kJ/m^2 for Level 1 mixtures. The SCB test has attracted growing interest from researchers in characterizing cracking resistance at intermediate temperatures due to its reliability [2, 3, 4].

While the SCB test effectively differentiates asphalt mixtures based on fracture resistance, its suitability for characterizing fatigue cracking resistance, as indicated by the J_c parameter, has been questioned [2, 3, 5, 6]. Fatigue tests under cyclic loading can better simulate the damage accumulation in asphalt pavements compared to fracture tests under monotonic loading. It is noted that the crack propagation generated in cyclic SCB tests is often modeled using Paris' Law to characterize the fatigue properties of asphalt materials [7, 8, 9].

The process of determining the Paris' Law coefficients in a crack propagation test, such as a cyclic SCB test, requires the measurement of the crack length. However, the crack length cannot be measured directly using conventional sensors, such as strain gauges, extensometers, or linear variable displacement transducers (LVDTs). Therefore, Digital Image Correlation (DIC) has been introduced to overcome this limitation. DIC is a non-contact optical-based technique used to measure the full-field 2D or 3D displacement and strain on the surface of a test specimen throughout a mechanical test [10]. Researchers have employed the DIC technique in asphalt mixture testing to investigate crack propagation in asphalt mixtures [11, 12, 13, 14]. DIC provides an innovative approach to investigating cracking phenomena and fracture characteristics in asphalt mixtures.

Although previous studies have explored cyclic SCB tests for the crack resistance characterization of asphalt mixtures, a standard cyclic SCB test method has not yet been established. For the purpose of developing a standard cyclic SCB test, there is a need to employ DIC for crack propagation characterization and investigate the optimal testing parameters of the cyclic SCB test.

Literature Review

Digital Image Correlation (DIC)

DIC is a non-contact optical-based technique to measure the full-field 2D or 3D displacement and strain on the surface of a test specimen during a mechanical test. Although DIC was introduced for material testing in the early 1980s [10], it has not yet been used to its highest potential in asphalt mixture testing. Instead, DIC is one of the emerging measurement technologies employed in asphalt pavement testing [15, 16, 17]. DIC has unique edges for investigating cracking phenomena and characteristics for a fracture test, as it provides detailed, spatially resolved information around the cracking areas in the specimen surface. Due to the development of advanced digital photography equipment, DIC has further potential as a reliable and convenient methodology for the fracture testing of asphalt mixtures.

Compared to conventional measurement techniques, such as the use of LVDTs, DIC has the following advantages:

- DIC provides full-field displacement and strain measurements of the specimen's testing surface;
- Because DIC is a non-contact measurement technique, it does not interfere with the subject and thus eliminates the need for mounting devices;
- Conventional instrumentation has deformation limitations, whereas DIC can be used to measure relatively large deformations; and
- DIC provides more post-processing options than conventional measurements.

Digital Photography

To monitor the mechanical responses, DIC uses digital cameras to capture images of the specimen surface. Digital cameras contain arrays of photoelectric sensors to capture, edit, or develop images. A single sensor element in photoelectric sensors is called a sensel. During the process of capturing digital images, a certain number of photons expose each sensel, causing it to output a corresponding range of voltage. This voltage eventually converts into a single value that represents the light intensity of the digital image.

A digital image can be considered as a matrix of individual cells called pixels. Each pixel stores a value or a set of values representing light intensity. A digital image is finite and discrete, and it can be analyzed quantitatively. For example, in an 8-bit grayscale image, pixel values range from 0 (black) to 255 (white), indicating varying light levels. This pixel matrix captures the light intensity patterns on a specimen's surface, as illustrated in Figure 1.

Figure 1. Digitization of light intensity

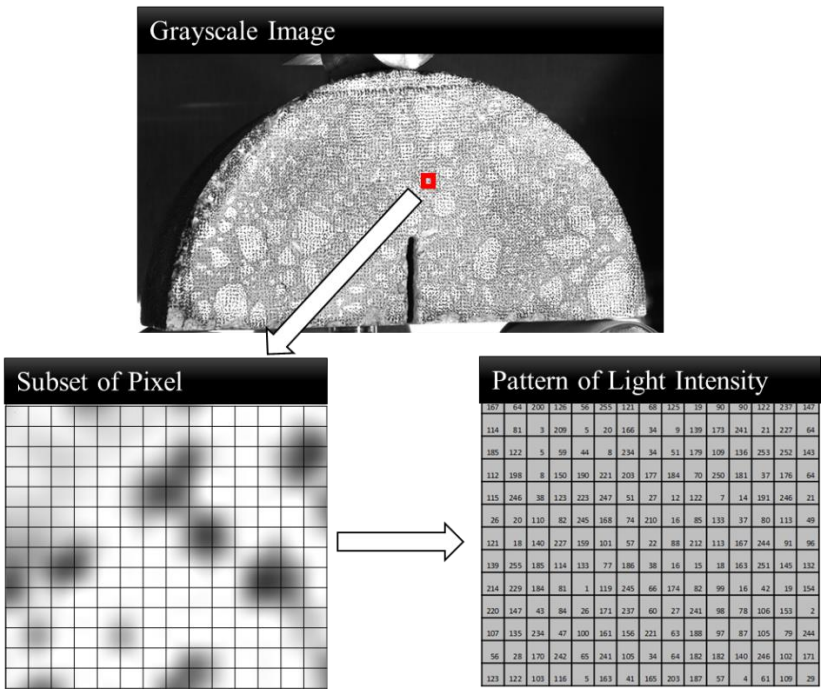

DIC Image Analysis

Through image analysis, DIC can monitor and calculate the displacements and strains along an object's surface. Consider a subset of digital images captured from the test surface. The reflected light intensity represented by pixel values from this surface consists of a light-intensity pattern, as illustrated in Figure 2. The basic assumption of DIC is that under certain lighting conditions, the undeformed and deformed patterns, $f(x,\ y)$ and $f^*(x^*, y^*)$, from the respective object surfaces are unique to the related surface and thus able to build one-to-one correspondence, where x and y are the coordinates of the surface. This assumption allows for the identification and tracking of the correlated small subsets of the undeformed and deformed images, thereby obtaining the displacements of these small subsets from the actual object surface.

Figure 2. Light intensity pattern between undeformed and deformed images

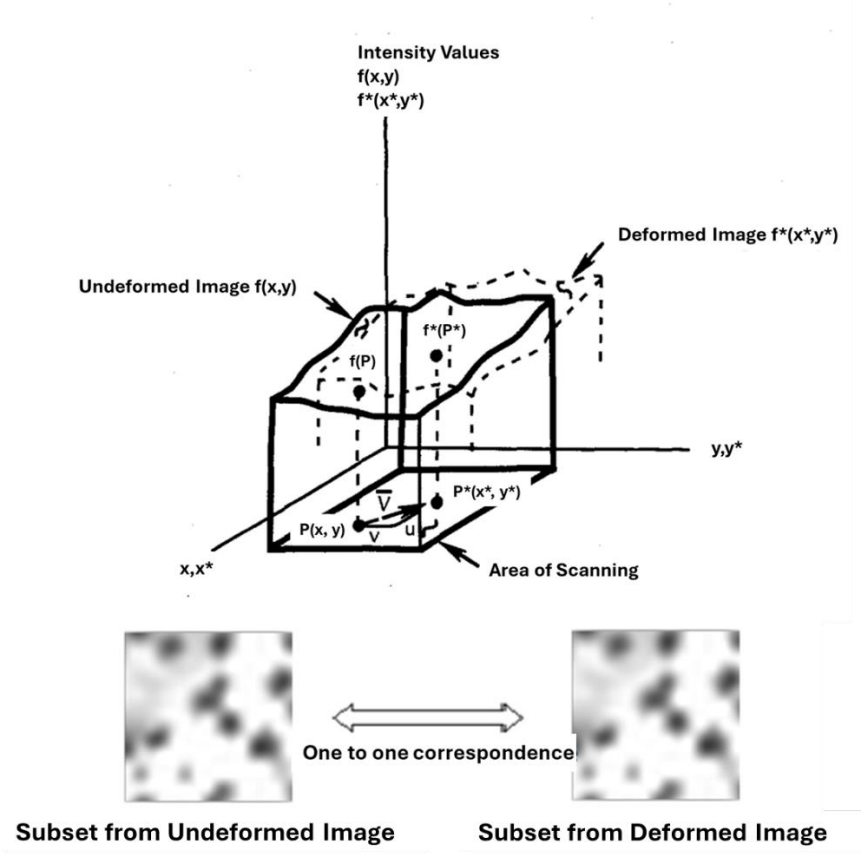

Consider a small subset of the surface centered at point *P*; if *Q* is any neighborhood point of *P*, then the light intensity values *f(P)* and *f(Q)* can be written to Equation 1 and Equation 2 [10].

$$f(P) = f(x,\ y,\ z) \tag{1}$$

$$f(Q) = f(x + dx,\ y + dy,\ z + dz) \tag{2}$$

After deformation, the light intensity values of P^* and Q^* can be expressed by Equation 3 and Equation 4 [10], where $u,\ v,\ w$ are components of displacement.

$$f^*(P^*) = f[x + u(P),\ y + v(P),\ z + w(P)] \tag{3}$$

$$f^*(Q^*) = f[x + u(Q) + dx,\ y + v(Q) + dy,\ z + w(Q) + dz] \tag{4}$$

According to linear Taylor's displacement functions, the $f^*(Q^*)$ can be rewritten to Equation 5 [10].

$$f^*(Q^*) = f[x + u(P) + \frac{\partial u(P)}{\partial x}dx + \frac{\partial u(P)}{\partial y}dy + \frac{\partial u(P)}{\partial z}dz + dx, y + v(P) + \frac{\partial v(P)}{\partial x}dx + \frac{\partial v(P)}{\partial y}dy + \frac{\partial v(P)}{\partial z}dz + dy, z + w(P) + \frac{\partial w(P)}{\partial x}dx + \frac{\partial w(P)}{\partial y}dy + \frac{\partial w(P)}{\partial z}dz + dz] \quad (5)$$

Thus, one can compute the positions of P^* and Q^* by assuming all displacement components. The displacement components can be determined by comparing them to measured P^* and Q^* and applying iterative numerical computation methods.

Monotonic Semi-Circular Bend Test

The monotonic SCB test with a single notch was first developed by Chong and Kuruppu [18] to obtain the stress intensity factor and fracture toughness for rock, concrete, and ceramic materials. This test has been favored by many researchers and practitioners due to the ease of sample preparation and simple testing procedure. Louisiana DOTD currently requires the use of the SCB test as part of its balanced mix design framework for paving asphalt mixtures. The standard SCB test is conducted at 25°C in accordance with ASTM D8044, "Standard Test Method for Evaluation of Asphalt Mixture Cracking Resistance Using the Semi-Circular Bend (SCB) Test at Intermediate Temperatures" [1]. The test standard requires the use of semi-circular specimens with three notch depths. During testing, the specimen is loaded monotonically with an actuator displacement rate of 0.5 mm/min. until fracture. The load and displacement values are continuously measured during testing and are used to compute the SCB J_c value, a measure of the energy required to propagate cracks in the mixture, as shown in Equation 6.

$$J_C = -\left(\frac{1}{b}\right)\frac{dU}{da} \quad (6)$$

where,
Jc = critical strain energy release rate;
a = notch depth;
b = specimen thickness; and
U = total strain energy up to failure.

The SCB test and the validity of the SCB J_c parameter have been widely investigated and verified. Krans et al. [19] employed notched and un-notched semi-circular geometries to evaluate the fracture characteristics of asphalt mixtures under static and cyclic loads. The SCB test was performed on specimens with a diameter of 100 mm and a thickness of 25 mm. The specimens had a notch depth of 29 mm and were tested at 0°, 20°, and 30°C temperatures. They recommended the SCB test as a suitable tool to determine the crack growth properties of bituminous materials. Further, static SCB was introduced as a measure for quality control, whereas cyclic SCB can be utilized for design purposes.

Mull et al. [20] employed the J-integral concept to characterize the fracture resistance of chemically modified crumb rubber asphalt pavements at 24°C. They used three notch depths (i.e., 25.4 mm, 31.8 mm, and 38.1 mm) and obtained fracture energy per unit thickness. Next, the slope of fracture energy per unit thickness versus notch depth was considered the critical strain energy release rate, or J-integral, J_c. Chemically modified asphalt pavements showed higher J_c values, indicating improved fracture resistance compared to control asphalt pavements.

Mohammad et al. [5] investigated the fracture resistance of polymer-modified asphalt pavements by means of the SCB J_c parameter. They showed that the SCB test can be used as a valuable tool to predict fatigue crack growth in asphalt mixtures. Additionally, Wu et al. [21] suggested that the SCB test is an effective tool for evaluating the fracture resistance of asphalt mixtures. The ease of preparing and testing SCB samples makes it a well-suited method for evaluating the fracture resistance of both laboratory-compacted samples and field cores [22]. Further, the SCB geometry and test setup are capable of characterizing different fracture modes of asphalt mixtures by simply adjusting the inclination angle of the notch or the space between the two supports [23].

Cyclic Semi-Circular Bend Test

The cyclic SCB test, coupled with fracture mechanic principles, has been explored in existing studies to evaluate the crack propagation properties of asphalt mixtures. Some of them used DIC to investigate tensile strain and the crack propagation characteristics of asphalt mixtures.

Hofman et al. used both the digital camera and mortar displacement methods to identify the crack length in the cyclic SCB test [24]. Huang et al. adopted a methodology to estimate effective crack length based on specimen deformation data. A series of finite element analyses was performed at various crack lengths to construct the relationship between specimen deflection and effective crack length [8].

Hassan and Khalid employed dimensions of 150 mm in diameter, 65 mm in thickness, and 15 mm in notch depth for testing at a temperature of 5°C [25]. The test was controlled using a haversine load waveform with a frequency of 1 Hz. Crack propagation was monitored using a digital camera that was operated at 20 Frames Per Second (FPS). Crack length was determined by counting the pixels from the start to the end of the crack, following the actual crack path. In their analysis, the authors first assumed the asphalt concrete was quasi-elastic and utilized the Paris' Law equation of stress intensity factor ΔK. For this purpose, the analytical solution to ΔK derived by Lim et al. [26] for brittle materials was used. They further explored the use of the Paris' Law of fracture energy ΔJ considering the viscoelastic nature of asphalt concrete, for which ΔJ was estimated using the approach proposed by Schapery [27].

Van Rooijen and De Bondt used the cyclic SCB test to evaluate the crack propagation properties of asphalt mixture overlays against temperature-induced reflective cracking. The test was conducted at a relatively low temperature of 0°C to address the West European conditions and was controlled using a haversine load waveform at a frequency of 30 Hz. The maximum load was selected with 40-55% of the failure load obtained from the monotonic test performed using the displacement control at 0.85 mm/sec. The minimum load was set at 10% of the maximum load. The test specimens were notched to a depth of 10 mm [28].

Zhang et al. developed a novel approach to estimate crack length based on crack mouth opening displacement (CMOD) during the cyclic SCB test. The crack length is manually tracked by visual inspection to establish a correlation with the CMOD measured by LVDTs. Crack length and CMOD exhibited a good correlation with a quadratic function. The Paris' Law equation was fitted based on an estimated crack length curve and further used to evaluate the performance of sulfur-extended asphalt mixtures. The authors concluded that the cyclic SCB test demonstrated promise as a test method for assessing fatigue cracking resistance [14].

Jiang et al. utilized DIC on a modified cyclic SCB test to evaluate the fatigue properties of asphalt mixtures. Rest periods of 0, 0.4, 0.8, and 1.2 sec. were added between fatigue loading cycles to evaluate the healing properties of mixtures. Various indicators, including fatigue life, total dissipated energy, secant modulus, average deformation growth rate, and average tensile strain, were investigated for cyclic loads with or without rest periods. DIC was used to measure the tensile strain at the bottom of SCB specimens by applying a virtual gauge for DIC image analysis. The results indicated that the stone matrix asphalt mixture exhibited similar fatigue properties but significantly superior healing potential compared to the dense-graded mixture utilizing the same binder [29].

Yuan et al. investigated the accumulated fatigue damage of specimens during cyclic SCB tests. The average strain level along the specimen surface was measured by DIC and used to develop a damage indicator for evaluating fatigue damage during the cyclic SCB test. By measuring the average strain in a defined region around the crack tip, the damage assessment incorporates the effects of both the main crack and any surrounding small secondary cracks. Additionally, the effects of speckle pattern and out-of-plane displacement on DIC results were quantitatively analyzed in this study [30].

Jiang-san et al. utilized the cyclic SCB test coupled with DIC to investigate the anti-fatigue performance of warm mix asphalt mixtures. The horizontal strain of data points along the specimen surface is measured by DIC and used for fatigue performance evaluation. A modified Chaboche fatigue model was proposed to describe the formation of fatigue cracks, which was based on the standard deviation of the strain value D_{Exx} of data points. It was found that D_{Exx} had a strong relationship with the number of loading cycles on a logarithmic scale. The coupling effects of salt solution concentration and freeze-thaw cycles on the anti-fatigue performance of warm mix asphalt were evaluated by the proposed model. It is found that the accumulation of fatigue damage of hot mix asphalt (HMA) is less obviously affected by freeze-thaw cycles than that of warm mix asphalt (WMA) [31].

Cheng et al. proposed a method to predict the fatigue life of asphalt pavements based on the cyclic SCB test incorporated with a DIC system. The cyclic SCB test was conducted at a loading frequency of 10 Hz and used various stress levels ranging from 0.2 to 0.5 times the monotonic SCB fracture strength. In order to obtain the crack length curve that was used for Paris' Law fitting, an innovative method was developed to identify the crack length curve during the fatigue test by employing a K-d tree algorithm and a cohesive zone model. The Paris' Law coefficient results were further used to predict the fatigue life of asphalt pavements. Compared to methods in previous studies, the method developed in this study improved the precision and accuracy of crack length identification, whereas there are two factors which contributed to errors in crack length identification. First, the shape of the crack path required manual labeling. Second, the strain threshold that was used to determine the crack point was estimated by a theoretical model [9].

Fatigue Cracking Characterization Based on Fracture Mechanics

The fatigue testing based on fracture mechanics is able to assess the fundamental properties of materials, which are inherent and extendable to new materials and technologies, such as mixtures with reclaimed asphalt pavement (RAP) and recycled asphalt shingles (RAS) [32,

33, 34, 35]. Fracture mechanics principles assume that materials are inherently flawed, and the fatigue life is the number of repeated loads to propagate a dominant crack.

In fracture mechanics, the fatigue damage in a material consists of three phases: the crack initiation stage, the stable stage for crack propagation, and the tertiary stage (i.e., failure stage). The second phase is considered to consume most of the fracture energy and occupy most of the fatigue life. Therefore, many models based on fracture mechanics have been developed for this phase. One of the most popular models is Paris' Law, which is shown in Equation 7 [7]. Paris' Law can also be represented by the stress intensity factor instead of fracture energy; see Equation 8 [7].

$$\frac{da}{dN} = A(\Delta J)^n \tag{7}$$

where,
a = crack length, mm;
N = number of loading cycle;
ΔJ = range of fracture energy; and
A and n = coefficients of Paris' Law equation.

$$\frac{da}{dN} = A(\Delta K)^n \tag{8}$$

where,
ΔK is range of stress intensity factor.

Paris' Law is an empirical crack propagation model that describes the relationship between cracking growth rate and stress intensity factor for various engineering materials. Paris' Law has been widely used in predicting the fatigue characteristics of engineering materials.

Objective

The objective of this study was to develop a standard cyclic SCB test coupled with a DIC technique for characterizing the crack resistance of asphalt mixtures at intermediate temperatures. The specific objectives of the study included:

1. Setting up the DIC configurations for the optimization of deformation and crack propagation measurements of samples during cyclic SCB testing;
2. Developing a standard cyclic SCB test method for characterizing the fatigue cracking resistance of asphalt mixtures; and
3. Investigating the fatigue model based on the Paris' Law coefficients for predicting the fatigue life of asphalt pavements.

Scope

In this study, the DIC system was acquired and set up for the optimization of deformation and crack propagation measurements of mixture specimens during cyclic SCB testing. A plant-mixed asphalt mixture was selected for optimizing the parameters of the cyclic SCB test. Various specimen notch depths (i.e., 15, 20, and 25 mm) and loading frequencies (i.e., 1, 5, and 10 Hz) were investigated to find an optimal combination that yields reasonable results with the lowest test variability. The parameters, number of cycles to failure, N_f, and Paris' Law model coefficients, n and $Log(A)$, were used for crack characterization. A sensitivity analysis was designed and conducted to further investigate whether the developed test protocol was effective in differentiating asphalt mixtures with different fatigue cracking resistances. The indicators, number of cycles to failure, N_f, and the Paris' Law coefficients, were used to evaluate cracking resistance. Three 12.5 mm limestone asphalt mixtures with expected distinct cracking resistance performances were prepared and evaluated using the proposed cyclic SCB test. An innovative method was developed to directly measure the crack length during the cyclic SCB test, and the measured crack length curve was used to determine the coefficients of the Paris' Law model. The Paris' Law coefficients obtained from the cyclic SCB test were further used in the preliminary application of the pavement fatigue model for subsequent prediction of the fatigue life of asphalt pavements.

Methodology

Digital Image Correlation (DIC) System Setup and Image Analysis

DIC Equipment

The DIC system used in this study was manufactured by Correlated Solutions [36]. The DIC system is comprised of the DIC cameras, a mounting system, a lighting system, and a data acquisition system; see Figure 3. The resolution of the DIC camera is 1920×1200 pixels. DIC cameras are high-resolution imaging devices that capture digital images of the specimen surface during mechanical testing. These images are then analyzed to measure displacements and strains with high accuracy. The mounting system securely holds the cameras in place and ensures precise alignment and stability during testing. This system is crucial for maintaining the consistency and accuracy of the captured images. The lighting system provides consistent and adequate illumination to the specimen surface, which is essential for obtaining clear and high-contrast images. The data acquisition system interfaces with the cameras and collects the image data in real time. This system processes the captured images and transfers them to the analysis software, where the DIC algorithms compute the displacement and strain fields [37].

Figure 3. DIC equipment

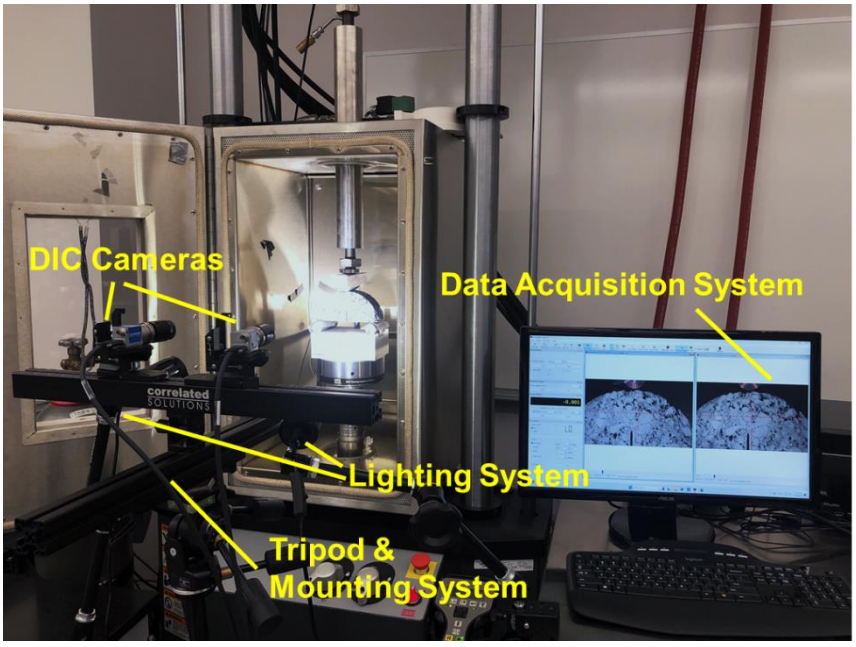

DIC Cameras Setup

The DIC setup aims to achieve two primary goals: accurate camera positioning and high-quality image capture. This is accomplished by carefully designing the camera angles and field of view (FOV) for each camera. Image quality in a DIC setup is influenced by several factors: speckle patterns, camera settings, and lighting conditions. Additionally, selecting the right frame rate is critical, as it helps to achieve a balance between the desired objective (i.e., capturing fast events) and the computational cost of image processing.

Stereo Angles

The stereo angles between the DIC cameras are critical for optimizing measurement accuracy; see Figure 4. Smaller stereo angles enhance the accuracy of in-plane displacement measurements. In contrast, larger stereo angles improve the accuracy of out-of-plane displacement measurements. The optimal stereo-angle range for most applications is between approximately 15° and 35°, balancing the accuracy of both in-plane and out-of-plane displacement measurements [36].

Figure 4. Illustration of stereo angle of DIC camera setup

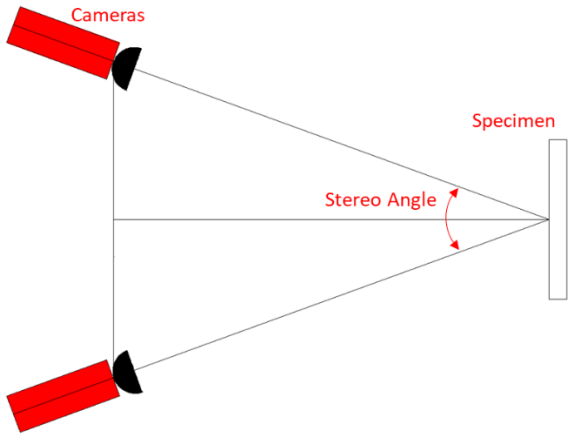

Fields of View (FOV) and Regions of Interest (ROI)

The field of view (FOV) refers to the total area that DIC cameras can capture. The size of the FOV is influenced by the lens focal length, the distance between the cameras and the specimen, and the camera sensor size. The FOV needs to be large enough to cover the object and its potential deformation. However, if the FOV is too large, it can reduce the spatial resolution, potentially compromising the accuracy of the detailed measurements within the captured area [37].

The region of interest (ROI) is a specific portion of the FOV that is selected during the analysis stage. The ROI is chosen based on the areas that are related to the study's needs. Usually, the FOV is determined by the needs of the ROI. By concentrating the ROI to meet the study needs, the FOV can be maintained in a concentrated area, allowing the analysis to achieve higher resolution and more accurate measurements in that specific region.

Determining the appropriate FOV and ROI requires balancing the need for comprehensive coverage with the need for detailed, high-resolution data. For example, in studies where the overall structural response is of interest, a larger FOV might be prioritized to capture global behavior. In contrast, for investigations focusing on specific failure mechanisms or small-scale deformations, a smaller FOV with a finely tuned ROI would be more appropriate [37].

Speckle Patterns

In some cases, the surface of the test specimen itself may have a sufficient natural pattern that is suitable for DIC, but most of the time, an artificially applied pattern is required on the specimen surface. Usually, white as the background color and black as the speckle are suitable for asphalt mixture specimens, as white is the most highly contrasted color to black binder.

The pattern density should be approximately 50%; that is, the areas of dark (black) and bright (white) should be approximately the same. The applied pattern should be of good quality (i.e., not fading, cracking, or debonding). The pattern sheen should be matte, not glossy, to avoid glare and specular reflection, as well as have a good bond with the underlying surface. It is important that the applied pattern be able to deform in accordance with the expected deformation of the test specimen. Specifically, for large deformation tests, the paint should be as ductile as possible. In contrast, cracking tests require brittle paint.

Camera Settings

The lighting conditions of the environment and the settings of the digital camera can affect the intensity value of a pixel. Lighting conditions are critical for achieving good image contrast in DIC setups. In most cases, additional lighting is necessary. It is recommended to avoid lighting that has significant intensity in the infrared range, as this may increase the temperature of the test piece. Cross-polarized light or diffuse light, rather than focused or spot light, is recommended to reduce the glare caused by specular reflections. The lighting intensity should be uniform throughout the testing time. A preferred contrast needs to be obtained by adjusting lighting conditions. Typically, at least 50% contrast (i.e., 130 counts for an 8-bit image) is preferred.

For camera settings, having a high dynamic range is desirable for photo sensors to produce quality images and obtain accurate DIC results, where the dynamic range of photo sensors in a camera is the difference between the highest and lowest intensity signals that the sensor can measure. Given a certain amount of input light, the pixel intensity value would be dependent on the following adjustable camera settings:

- **Gain (ISO).** Gain refers to the amount of voltage change that is produced after a given photon becomes stuck. More gain can help offset the effect of low light, whereas too much gain can increase the noise in the image.
- **Focus.** Adjusting the focus of a digital camera refers to changing the lenses' position or configuring the lenses' focus ring to ensure that the subject appears sharp and clear in the image. For DIC applications, the distance between the lens and the object is usually fixed, so the lens is typically focused manually prior to the test. Automatic focus functions, if any, should be banned, or they may negatively affect the accuracy of DIC results.
- **Aperture.** The aperture regulates the amount of light entering the camera, allowing for the adjustment of the light condition. Additionally, aperture setting can also affect the depth of field of the image; smaller aperture openings have larger depths of field.
- **Shutter.** Shutter controls the amount of time the camera allows the light to pass through to produce an image. Longer shutter times can help offset the effects of low lighting, but too much shutter time would cause a blurry image and reduce the accuracy of results when significant movement or deformation happens between individual images.

Lighting Condition

Most of the time, additional lighting is necessary to achieve adequate contrast for a given aperture and exposure time. Proper lighting minimizes shadows and reflections that can interfere with image analysis. The intensity offered by the lighting system should be uniform throughout the test. Adjust lighting to obtain a preferred contrast from images and to ensure no ROI of the image is overexposed or underexposed.

Frame Rate

Setting the frame rate appropriately is crucial in terms of the test objective and the computational cost of image processing. The frame rate is the number of frames captured per second, which determines how frequently images are taken during the experiment. A higher frame rate provides more detailed temporal resolution, which is essential for capturing fast, dynamic events and accurately analyzing rapid deformations or transient phenomena.

However, this also results in a larger volume of data, increasing the demands on storage and processing capabilities. Conversely, a lower frame rate reduces the data load and associated processing costs, making it suitable for tests with slower cumulative deformation, such as the cyclic SCB test, in which high temporal resolution is not required. Selecting the appropriate frame rate involves balancing the need to capture sufficient temporal detail with practical considerations of data management and processing resources.

DIC Image Processing

After the test is complete and the DIC images have been captured, the subsequent step involves processing these images to derive essential data, such as deformation and strain. In this study, the dedicated software VIC-3D [36] was employed for image processing. The image analysis workflow encompassed several key stages, including selecting a reference image, delineating the region of interest (ROI), conducting image correlation, and computing strain.

In the process of image correlation analysis, the DIC algorithm tracks the motions occurring between the reference image and subsequent deformed images. The subsets delineated on the reference image serve as the initial reference points for motion tracking. For a mechanical test using repeated loading, selecting a reference image obtained after the first few cycles has been found to be the proper choice. At this point, the responses from the specimen have been stabilized, and the fatigue damage has not accumulated.

The next step is selecting ROI, where image correlation is going to be processed. The ROI can be selected as an entire image or a portion of an image. With the fixed FOV, selecting different sizes of ROI will not change the spatial resolution of displacement or strain results. However, a proper selection of ROI can significantly optimize computational resources and disk space usage, thus enhancing efficiency without compromising the accuracy of the analysis.

Once the reference image and ROI have been selected, the image correlation and subsequent strain calculation can be conducted. The principles of image correlation and displacement/strain calculation have been stated in the Literature Review section above. In this study, the image processing was conducted using the software VIC-3D, which comes with the DIC system from the same manufacturer. There are three important parameters for this processing:

- **Subset Size.** Subset size is the size of mesh that is applied across the image to build the one-to-one correspondence of speckle patterns within each subset. Therefore, a unique point for each subset can be identified and used to track each subset before and after deformation. The subset size is user-defined and depends on the speckle size. The size should be large enough to have a unique speckle pattern within it. However, if the subset size is too large, it will result in poor resolution.
- **Step Size.** The step size refers to the distance between neighboring subsets used in correlation analysis. The step size is the offset by which the algorithm completes one track of a subset and moves to the next. While the subset size determines the spatial resolution, the step size influences the density of data points in the measured displacement and strain fields. A smaller step size results in a higher density of data points, providing a more detailed and continuous representation of the deformation, but it also increases computational effort and processing time.
- **Strain Filter Size.** The strain filter is used to average the strains over a number of data points from neighboring areas. For example, a strain filter size of "5" means it averages the strains over 5×5 data points. Note that the size of the strain filter is expressed in terms of data points instead of pixels for subset size or step size. The selection of strain filter size represents how many data points are used for strain computation. Small strain filters provide better resolution and more localized data. However, large strain filters increase the accuracy of strain because they contain information from more data points and therefore have less uncertainty.

DIC Test Procedures and Configuration for Cyclic SCB Test

The steps for conducting a DIC-coupled SCB test are as follows:

- Apply a speckle pattern to the SCB specimens;
- Place and set up cameras in the desired positions;
- Take calibration images and run DIC calibration;
- Start the mechanical test and capture images at the same time; and
- Run image processing and perform image post-processing analysis.

The following sections provide the specifics of the procedures and configurations for each of these steps.

Applying Speckle Pattern

The speckle pattern of white background and black speckle was applied to the surface of the SCB test specimens. Ensuring speckle quality in terms of image contrast and dot size is important for accurate DIC analysis. To achieve optimal speckle quality, a matte paint was employed to generate a white background on the specimen surface. This matte paint was specifically chosen for its ability to provide a uniform, non-reflective surface, ensuring consistent speckle contrast across the specimen. The paint was sprayed onto the specimen surface to ensure uniform coverage and adherence. It is important to ensure that tests are performed on specimens with fully dried matte paint.

For the best performance of DIC algorithms, the desired speckle dot size is three to five pixels [37]. If the pattern feature is too small, it could be aliased and added as an error to DIC results. If the pattern feature is too large, it will require larger subsets and thus degrade the spatial resolution. Considering the application of SCB specimen size and camera setup, the dot size of the speckle pattern was selected as 0.33 mm, based on manufacturer's recommendations; see Table 1. A speckle stamp was used to produce a speckle of black dots; see Figure 5.

Table 1. Recommendation of DIC speckle dot size

Field of View	Dot Size					
	0.18 mm	0.33 mm	0.66 mm	1.27 mm	2.54 mm	5.08 mm
1 MP Camera 1024 pixel	2.3-6.1 cm	4.2-11 cm	8.4-23 cm	16-43 cm	33-87 cm	65-173 cm
2.3 MP Camera 1920 pixel	4.3-11 cm	7.9-21 cm	16-42 cm	31-81 cm	61-163 cm	122-325 cm
5 MP Camera 2448 pixel	5.4-15 cm	10-27 cm	20-54 cm	39-103 cm	78-207 cm	155-415 cm
16 MP Camera 4872 pixel	11-29 cm	20-54 cm	40-107 cm	77-206 cm	155-413 cm	309-825 cm

Figure 5. Speckle stamp and SCB specimen with speckle pattern

DIC Camera Setup

Before calibrating DIC, the cameras, mounting systems, and lighting systems were positioned and set up. The trial images were then taken to check the applied pattern and image quality, as well as the light conditions. The stereo angle of the cameras was maintained at 15° to 35°. The distance between the cameras and specimen was adjusted to obtain an appropriate field of view (FOV); see Figure 6. A good use of the field of view (FOV) should

strive to maximize the occupation of the region of interest (ROI) within the image, thereby leveraging the full potential of the camera's resolution.

Figure 6. Field of view (FOV) for SCB specimen: (a) too far and (b) a good use

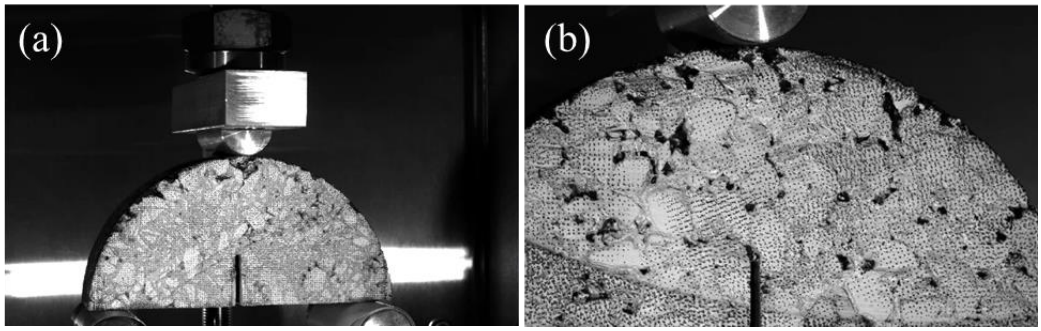

(a) Too Far **(b) A Good Use**

DIC Calibration

The DIC calibration process is a critical step to ensure the accuracy and reliability of deformation and strain measurements obtained from DIC analysis. The first step is to adjust the camera settings, as well as the lighting conditions, to capture quality images. The adjustable camera settings encompass intrinsic parameters such as focal length, aperture, shutter speed, and lens distortion coefficients. These parameters, along with gain, are calibrated to ensure optimal image quality. Verification is then performed using VIC-3D software.

The next step is to capture the images of a calibration target with known geometric features using the VIC-3D software, followed by the extraction and analysis of the calibration data. This calibration procedure involves establishing a relationship between the movement of points in the DIC images and the corresponding physical displacements in the specimen. A series of images of the calibration target are taken and used for calibration analysis. At least 30 images with a good range of tilt should be acquired for the calibration. A calibration score of less than 0.1 is desired for accurate results. Figure 7 shows the calibration target and VIC-3D interface.

Figure 7. Calibration target and software interface for DIC calibration

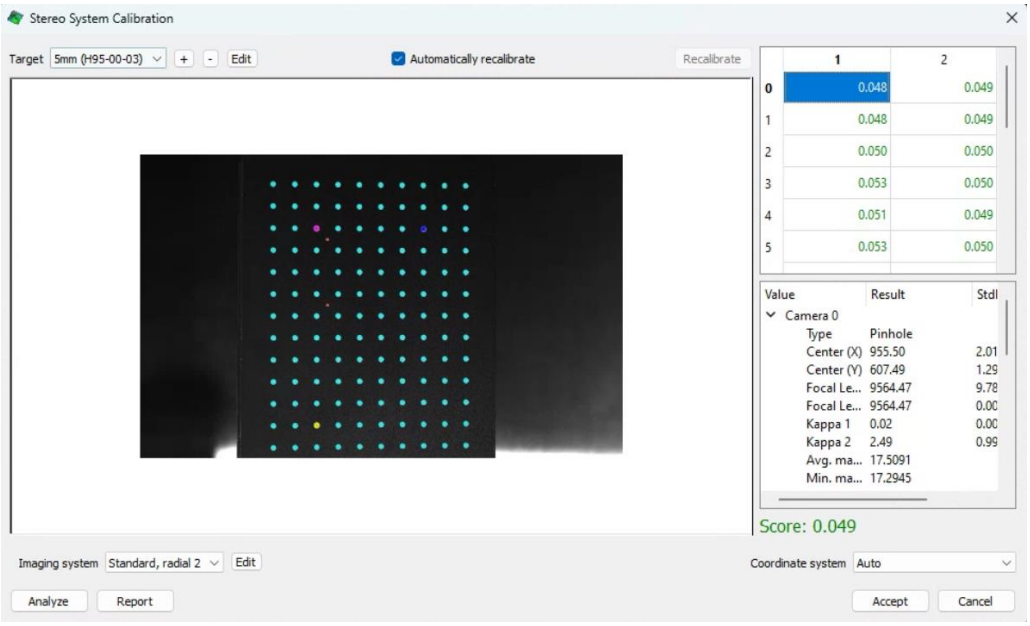

DIC Image Capture

While running the cyclic SCB test, the DIC system starts to capture images simultaneously. The image acquisition rate for the cyclic SCB test was configured to one image per second, considering a balance between effective measurement and computation cost while ensuring adequate capability for cumulative damage assessment. For the purpose of the developed approach in this study, additional undeformed images were captured before starting the test.

Image Correlation Analysis and Post-Processing Analysis

The final step is to run an image correlation analysis and strain calculation. The VIC-3D software imports the calibration data and the captured DIC image sequences for analysis. Figure 7 shows the region of interest (ROI) for the DIC image analysis. It is a rectangle with a height equal to the specimen's height and a fixed width of 40 mm. This specific area was chosen because it is where cracks are most likely to occur.

Figure 8. Region of interest (ROI) for DIC analysis

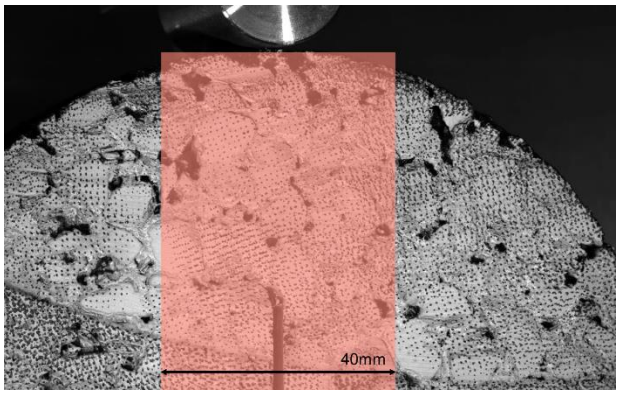

As stated in the previous section, there are three parameters in image correlation analysis: subset size, step size, and strain filter size. VIC-3D performs image correlation analysis by comparing subsets between the reference and deformed images to calculate displacement fields. Users define the subset size within images to conduct image correlation analysis, enabling the monitoring of displacement in ROI between the reference and deformed images. Additionally, users define the step size as the spacing of output data points. Following the displacement field analysis, strain fields are computed using numerical differentiation methods, which offer valuable insights into the behavior of material deformation. The strain filter size is defined as the number of data points in the displacement field for computing strain. In this study, a subset size of “25,” a step size of “2,” and a strain filter size of “5” were utilized. These parameters have been optimized specifically for the developed analysis methodology in cyclic SCB testing.

Development of Cyclic SCB Test Protocol

Selection of Testing Parameters for Cyclic SCB Test

The following sections explore several key variables that influence the results of cyclic SCB tests. These variables include specimen geometry, loading level, and loading frequency. Table 2 presents a summary of the literature review on key variables used in cyclic SCB tests from previous studies. The cyclic SCB test was conducted in stress-controlled mode, where the maximum load within a cycle (i.e., stress level) is constant. The stress level of the load is critical for stress-controlled fatigue testing. Using the same stress level for asphalt mixtures with different tensile strengths may lead to an overestimation of fatigue life for high-strength mixtures, or vice versa. Generally, the stress ratio, a proportional value of the tensile strength, serves as the stress level for the fatigue test. The SCB specimen's geometry includes notch depth and thickness. A review of relevant literature led to the selection of a thickness of 50 mm for this study.

Table 2. Summary of literature review on testing parameters for cyclic SCB test

Reference	Temperature, ℃	Load Level	Thickness, mm	Notch Depth, mm	Load Frequency, Hz
Huang et al. [8]	25	1.45kN	48	25	5
Hassan, M. M. [25]	5	1.5kN	65	15	1
Saha et al. [38]	15	50 με of CMOD	50	15	10
Jiang et al. [29]	15	1 - 3kN	50	0, 15, 25	10
Yuan et al. [30]	15	0.2-0.5 times of tensile strength	50	15	10

Experiment Program and Materials

Experiment Program

Two experiment programs were designed for this study; the first program aimed to optimize testing parameters such as sample notch depth and load frequency, and the second focused on a sensitivity analysis of the proposed testing protocol. First, a full factorial design was conducted to investigate the effects of sample notch depth and load frequency on the cyclic SCB test. Three notch depths (i.e., 15, 20, and 25 mm) and loading frequencies (i.e., 1, 5, and 10 Hz) were considered for this study. The factorial design of the test program included

combinations of three levels of notch depth and three levels of loading frequency, for a total of nine groups. A set of monotonic SCB tests was conducted to determine the SCB strength prior to conducting cyclic SCB tests for each group. Four replications were conducted for each group of monotonic SCB and cyclic SCB tests, respectively.

Second, three 12.5 mm limestone asphalt mixtures with expected distinct cracking resistance performances were prepared and evaluated using the cyclic SCB test protocol for the sensitivity analysis. The Paris' Law coefficients, along with other indicators, were used for the evaluation of cracking resistance. Additionally, the standard SCB-J_c tests were conducted to obtain J_c, and the SCB-J_c results were compared for sensitivity analysis. Additionally, dynamic modulus tests were conducted for these mixtures. Dynamic modulus data was used for models used to predict the fatigue life of asphalt pavements.

Materials

A 12.5 mm nominal maximum aggregate size (NMAS) plant-produced asphalt mixture prepared with styrene-butadiene-styrene (SBS) modified PG 70-22 and limestone aggregates was selected for the experimental program to optimize test parameters. This mixture, designated HMA 12.5, contained liquid anti-strip additive at a dosage rate of 0.6% by weight of mixture and 19% RAP material; see Table 3. Three 12.5 mm NMAS limestone asphalt mixtures with distinct cracking resistance performances were prepared and evaluated using the cyclic SCB test for the experiment program and sensitivity analysis. These mixtures included asphalt mixtures prepared with PG 76-22M (best cracking resistance, 76R0 in Table 3), PG 70-22M and 30% reclaimed asphalt pavement (RAP) (intermediate cracking resistance, 70R30 in Table 3), and PG 67-22 and 50% RAP (worst cracking resistance, 67R50 in Table 3). The gradations of mixtures 70R30 and 67R50 were adjusted to be similar to that of 76R0. To achieve a similar aggregate distribution for the three mixtures, the gradation of the RAP material was first determined. Next, the gradations of mixtures 70R30 and 67R50 were adjusted by changing the proportions of other aggregates to ensure their gradation was similar to that of mixture 76R0, with no RAP included. This adjustment ensured compliance with the requirements specified in the Louisiana DOTD's Standard Specifications for Roads and Bridges, Table 502-4 [39]. Figure 9 presents the aggregate gradation of the mixtures used in this study.

Table 3. Mixture design properties

Mixture Design Properties	HMA12.5	76R0	70R30	67R50
Binder grade	PG70-22	PG76-22	PG70-22	PG67-22
RAP percentage, %	19	0	30	50
Asphalt content, %	5.1	5.3	5.3	5.3
Air voids, %	3.5	3.9	3.9	3.6
Voids in mineral aggregate, %	13.8	14.8	14.9	14.9
Voids filled with asphalt, %	75	74.2	74.6	76
Maximum specific gravity	2.476	2.476	2.458	2.442
Effective specific gravity	2.678	2.684	2.663	2.654
Percent absorbed asphalt, %	0.68	0.57	0.40	0.39
Effective asphalt content, %	4.4	4.8	4.9	4.9

Figure 9. Aggregate gradation of asphalt mixtures

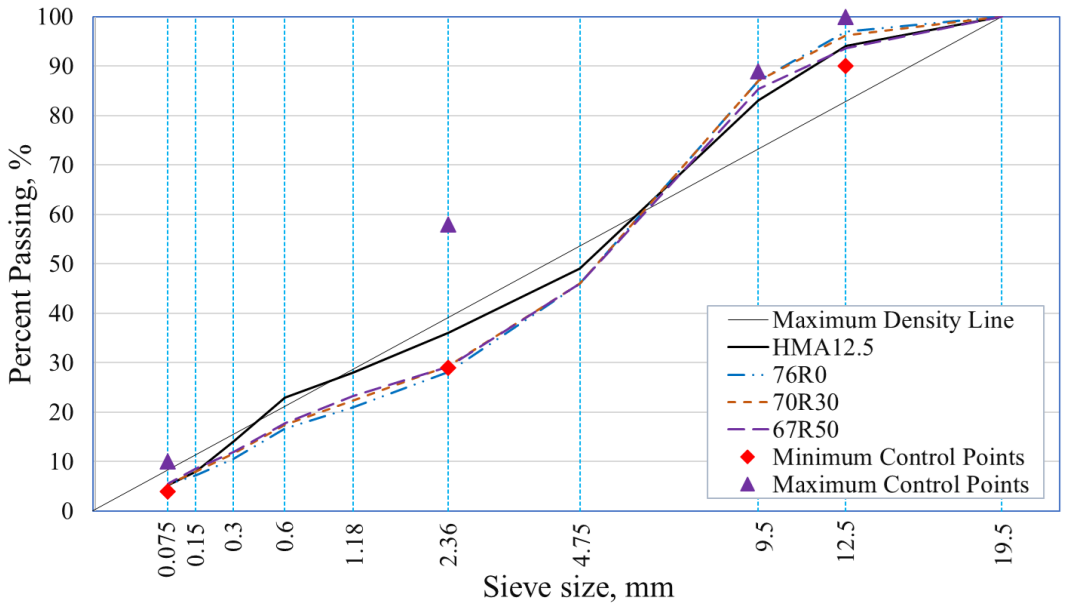

Testing Methods

SCB Specimen Preparation

The specimens for SCB tests were compacted using the Superpave gyratory compactor at a temperature of 140°C according to ASTM D6925, "Standard Test Method for Preparation and Determination of the Relative Density of Asphalt Mix Specimens by Means of the Superpave Gyratory Compactor." Figure 10 presents the scheme of SCB sample preparation. DIC requires a smooth test specimen surface for applying speckle patterns. Therefore, the SCB samples were prepared by cutting them from a larger specimen to achieve the required smoothness. First, a cylindrical specimen with a 150 mm diameter and 150 mm height was compacted and sliced into two identical disks with the desired thickness. To create smooth surfaces for applying speckle patterns, both ends of each cylindrical specimen were removed. This process also minimized variations caused by air voids. In the next step, each disk was cut into two semi-circular samples, each of which was notched to the desired notch depth. The air void contents of the specimens were maintained within 7±0.5%.

Figure 10. Scheme of SCB sample preparation

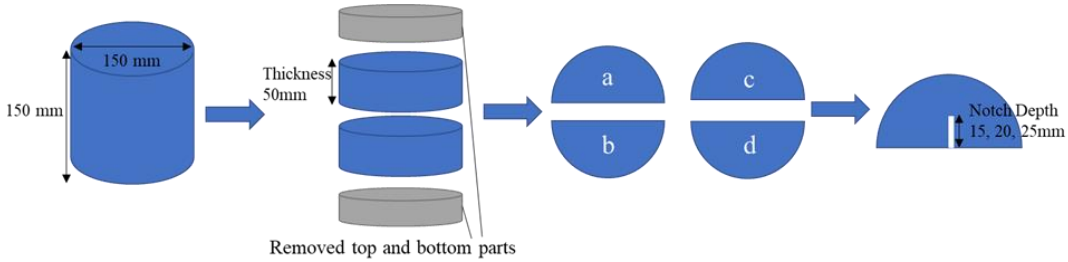

Monotonic SCB Test

The monotonic SCB test was conducted according to ASTM D8044 [1] to evaluate the intermediate-temperature cracking resistance of asphalt mixtures. After compaction, the samples were cut, notched, and subjected to oven aging prior to testing. The test was performed at a constant displacement rate of 0.5 mm/min at 25°C. The critical strain energy release rate, J_c, was used to ascertain the cracking resistance of the asphalt mixtures. The critical strain energy release rate, J_c, was calculated using Equation 6. All test specimens were subjected to oven aging at 85°C for 120 hours in accordance with AASHTO R30 prior to testing [40].

Cyclic SCB Test

The test setup for cyclic SCB is depicted in
Figure 11. Fatigue loading was applied at the mid-point of the specimen arch by a loading strip, which was supported by two rollers at the bottom edge of the specimen. The space between the two supporting rollers was 120 mm. A sinusoidal load with a constant maximum peak load was used as fatigue loading. The value of the maximum peak load was determined by multiplying the SCB strength by a fatigue ratio value accordingly. Prior to conducting the cyclic SCB test, a series of monotonic SCB tests was conducted to determine the SCB strength, which is defined as the peak load recorded during these tests. A fatigue ratio of 0.5 was used. During the cyclic SCB test, the DIC system initiates the capture of images simultaneously. The image acquisition rate for the cyclic SCB test was configured to one image per second, considering a balance between effective measurement and computational cost while ensuring adequate capability for cumulative damage assessment.

Figure 11. Cyclic SCB test

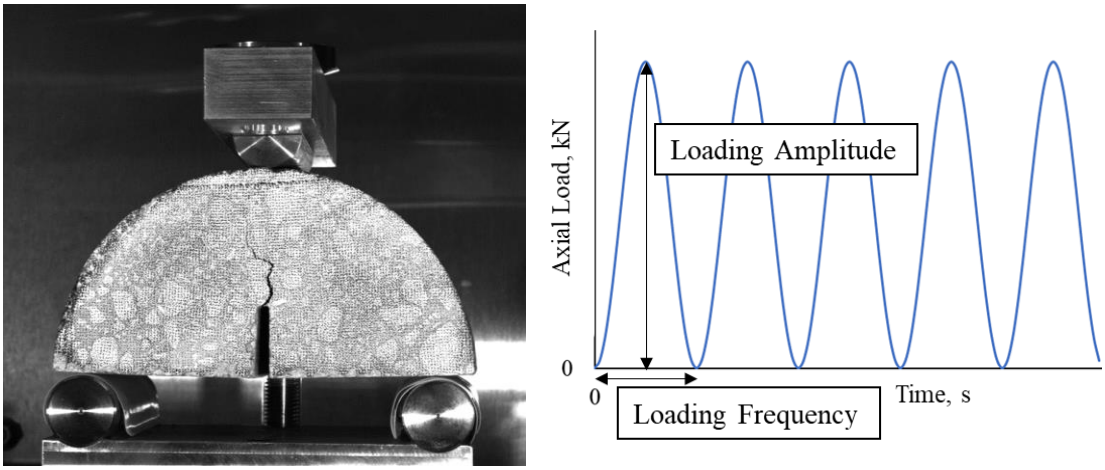

(a) Test Setup **(a) Fatigue Loading**

Cracking Resistance Evaluation of Asphalt Mixture Based on Cyclic SCB Test

Number of Cycles to Failure

Figure 12 presents a typical fatigue curve of load-line displacement (LLD) versus number of cycles during the cyclic SCB test. The figure also includes a derivative curve of LLD, plotted on a logarithmic scale. The fatigue curve of the cyclic SCB test can be divided into three stages: the initial stage, stable stage, and tertiary stage. In the initial stage, cracks developed rapidly, while in the stable stage, the propagation rate of cracks became relatively stable. After the stable stage, the crack propagation rate increased significantly, which marked the

failure point of the tertiary stage, characterized by unstable crack growth resulting in failure. The number of cycles to failure, N_f, is defined as fatigue cycles at the failure point, which is the transition between the stable stage and the tertiary stage. As the derivative of LLD is correlated to crack propagation, the failure point can be recognized based on the derivative of LLD. Specifically, the failure point is identified as the moment when the derivative of LLD exceeds a threshold value. In this study, a threshold of 1% for the maximum derivative value of LLD was used. The N_f is calculated as the number of fatigue cycles where the derivative of LLD exceeds the threshold value. It is noted that although other significant levels can be used, they would not significantly affect the N_f results.

Figure 12. Fatigue curve illustration from cyclic SCB test

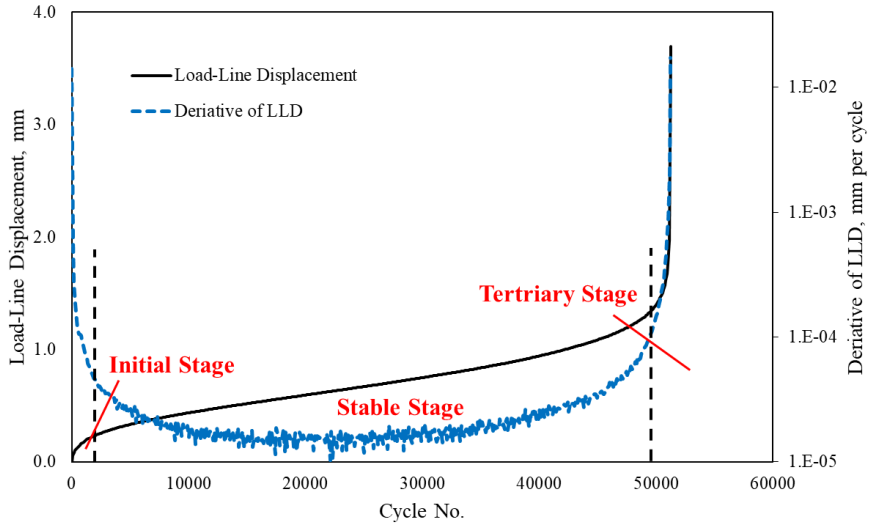

Paris' Law Coefficients

While running the cyclic SCB test, the DIC system was started to simultaneously capture images of the SCB sample to monitor crack propagation during testing. The DIC is used to analyze the deformation and displacement of the surface of SCB samples by comparing digital images captured before and during loading.

Figure 13 shows an example of the horizontal strain distribution on the SCB sample surface during the cyclic SCB test at different loading cycles of 10, 30, 50, 70, 90, and 99% of N_f, where positive strain values represent tensile strain. Considering that the values of vertical strain *eyy* and shear strain *exy* are negligible compared to horizontal strain *exx*, the *exx* was selected for display. High values of tensile strain are observed around the crack tip. Since the fracture energy dissipated after the specimen cracked, low strain values were in the areas

around the cracked path; see Figure 12. A key advantage of DIC in fracture testing is its ability to measure the entire crack length directly from the image. The crack length in the cyclic SCB test is defined as the distance measured along the loading direction (i.e., vertical) from the tip of the main crack to the bottom edge of the sample notch. In DIC image analysis, the length coordinates in mm of each pixel can be measured for both undeformed and deformed images. Thus, the crack length can be determined by visually inspecting the coordinates of the crack tip.

Figure 13. Strain distribution on SCB sample surface based on DIC analysis

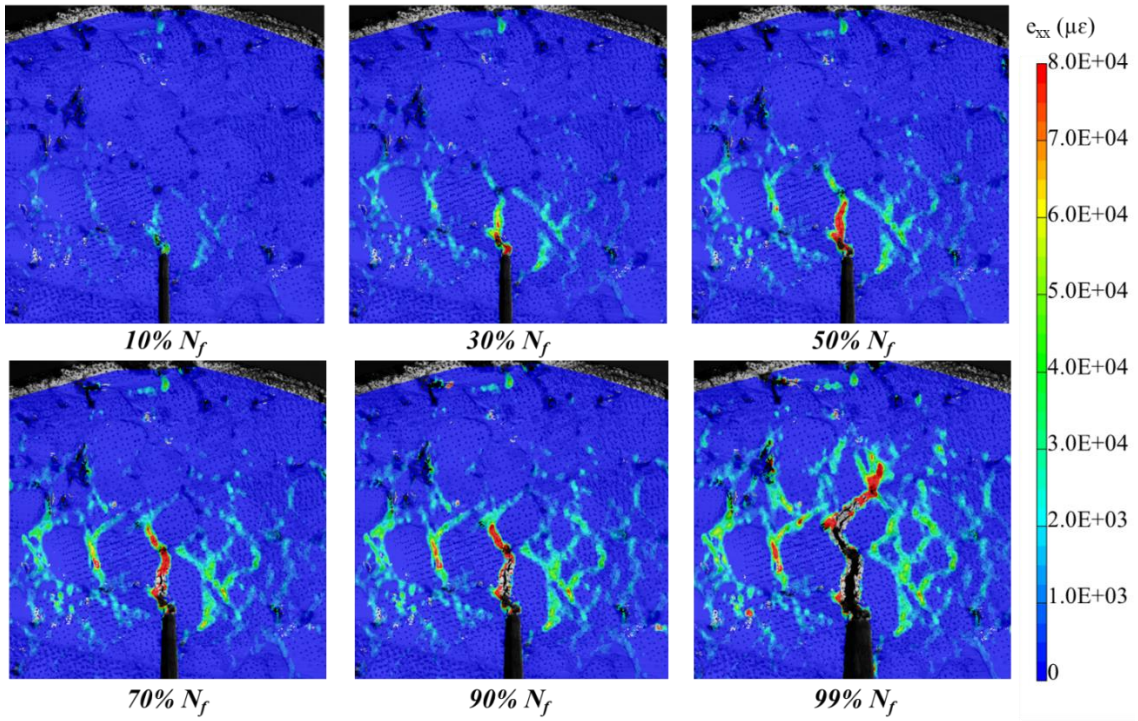

Although the crack length of one frame can be identified by visual inspection, obtaining the crack length curve throughout a fatigue test is extremely laborious. Zhang et al. reported that the crack mouth opening displacement (CMOD) can be used to estimate the crack length curve, as there exists a quadratic relationship between crack length and CMOD [14]. The establishment of a quadratic relationship only requires a few observations of CMOD and crack length points. In this way, the crack length curve during a cyclic SCB test can be estimated using the CMOD curve, while the CMOD curve can be measured by DIC with good precision and efficiency.

In the cyclic SCB test, DIC image analysis is utilized to measure the CMOD curve during testing. DIC analysis software, VIC-3D, was used to obtain CMOD by placing a virtual extensometer across the notch of the specimen. The CMOD value was measured as the distance between two reference points on either side of the notch. The CMOD measurement using the DIC virtual extensometer was validated utilizing a real clip-on extensometer, which was installed on the opposite side of the SCB specimen away from the camera; see Figure 14. Next, the CMOD curves measured using both the DIC virtual and real extensometers were compared. The results showed excellent agreement between the two sources, with a maximum error of only 0.1 mm. This confirms that DIC image analysis can accurately measure the CMOD curve.

Figure 14. Validation of CMOD measurement based on DIC

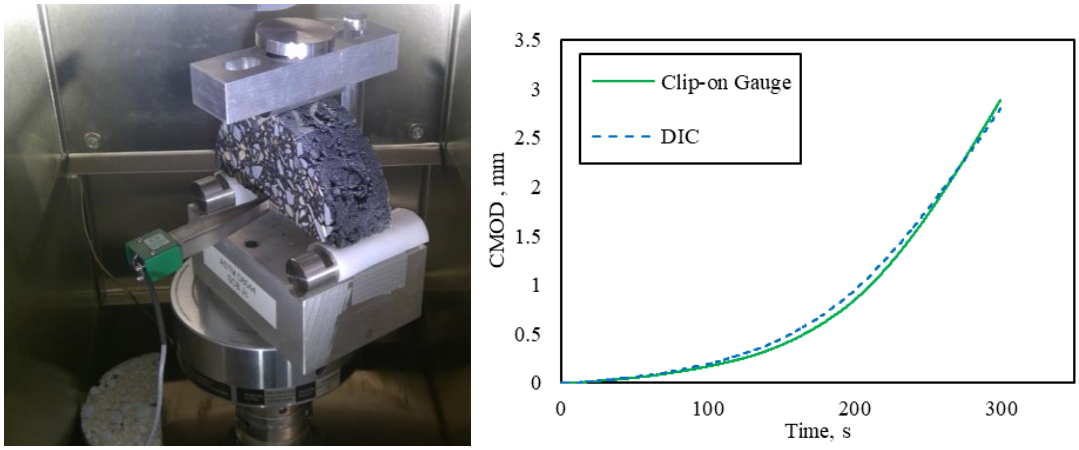

(a) Clip-on Extensometer **(b) Comparison Results of CMOD Measurement**

Figure 15 presents an example of the analysis process for crack length estimation. First, the CMOD curve was obtained from the DIC analysis. Next, the quadratic relationship between CMOD and crack length was established from quadratic fitting using 40 data points, while the CMOD-associated values of crack length were obtained from visual inspection. Finally, the crack length curve was estimated by substituting the CMOD curve into the quadratic relationship. It is noted that the visual inspection points were uniformly selected from the log scale range of loading cycles in order to obtain an unleveraged data set.

Figure 15. Crack length curve estimation based on DIC

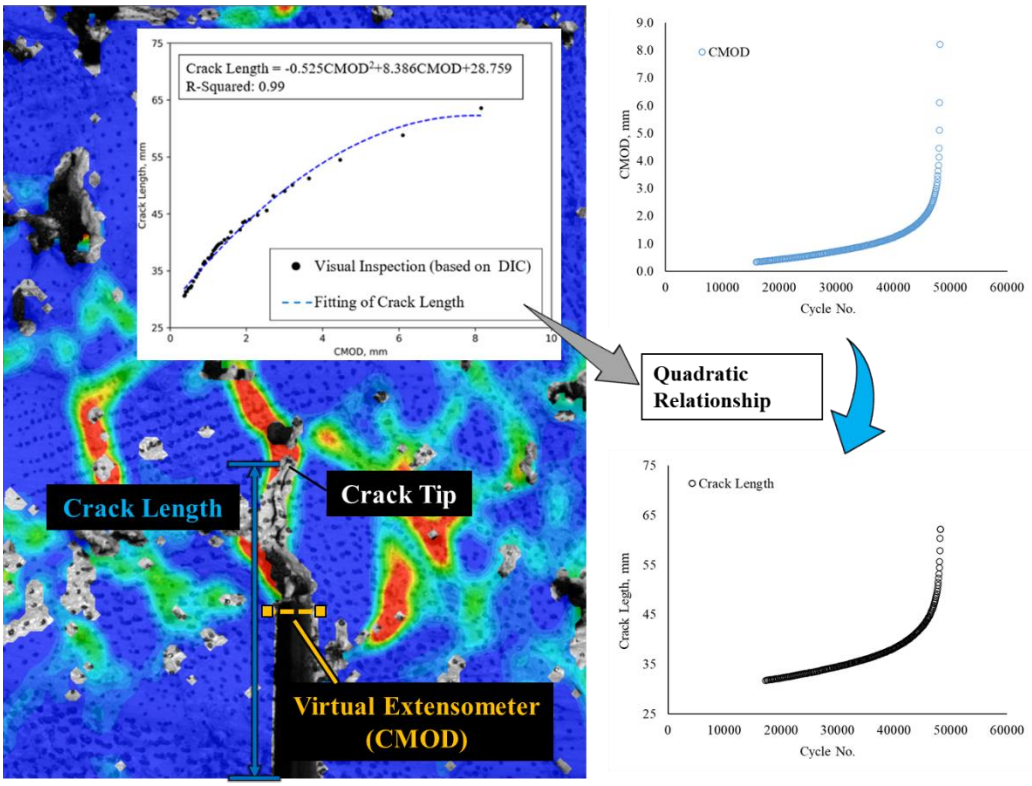

The coefficients *n* and *Log(A)* of the Paris' Law equation were used to characterize the fatigue cracking resistance of asphalt mixture. The estimated crack length curve based on CMOD was used for fitting the Paris' Law equation. Paris' Law describes the relationship between cracking growth rate and stress intensity factor for various engineering materials. When the contact stress applied is very small, the stress intensity factor *(*ΔK*)* can be approximated by the stress intensity factor at the maximum load (K_I) during the loading cycle. For a semi-circular specimen, the value of K_I can be calculated as shown in Equations 9 to 11 [26].

$$K_I = Y_{I(0.8)}\sigma_0\sqrt{\pi a} \tag{9}$$

$$\sigma_0 = P/2rt \tag{10}$$

$$Y_{I(0.8)} = 4.782 + 1.219(\frac{a}{r}) + 0.063\,exp(\,7.045(\frac{a}{r})) \tag{11}$$

where,

a = crack length (including notch depth), m;

K_I = the stress intensity factor at maximum load, kN·m-1.5;

$Y_{I(0.8)}$ = the normalized stress intensity factor;

P = the amplitude of cyclic load, kN; and

r and t = the specimen radius and thickness, respectively, m.

Figure 16 shows an example of crack length data fitted to Paris' Law. For smoothing purposes, the crack growth rate, da/dN, was calculated from 200 intervals of the crack length curve on the log-log scale. Paris' Law describes a linear relationship between crack growth rate and stress intensity factor on a log-log scale, where *Log(A)* is the intercept and *n* is the slope. The coefficients *Log(A)* and *n* describe the crack growth rate for ΔK equal to one and the susceptibility of the cracking growth rate to change in stress intensity factor, respectively. The evaluation of the fatigue cracking resistance of asphalt mixtures should be interpreted by both coefficients, *Log(A)* and *n*. It is worth mentioning that asphalt mixtures with lower *n* and/or lower *Log(A)* values are desirable for enhanced cracking resistance.

Figure 16. Paris' Law fitting

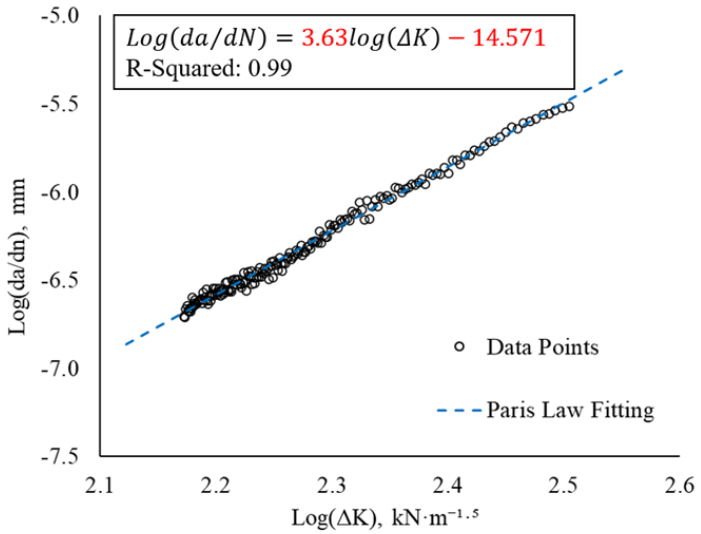

An Innovative Method for Crack Length Identification During Cyclic SCB Test

In order to determine the Paris' Law coefficients in a crack propagation test, the key challenge is identifying the crack length that initiated and propagated within the specimen. However, existing methodologies, such as the CMOD-based method described in the previous section, rely on indirect approaches and manual labeling during the analysis process, which limits the efficiency and scalability of DIC. In this section, an innovative approach based on DIC confidence margins (i.e., *sigma*) was developed to directly recognize crack length. The crack length identified by the developed approach can be used for the determination of the Paris' Law coefficients for the cyclic SCB test. The following sub-sections describe this approach in detail.

Confidence Margins of DIC Image Analysis

In DIC image analysis, an iterative numerical algorithm was used to match the reference image (i.e., undeformed) to the deformed image. To assess the matching errors arising from numerical computation, the confidence margins (i.e., *sigma*) can be utilized to evaluate the level of error incurred during the matching process [37]. Crack propagation induced by fatigue loading during cyclic SCB testing results in damage to the speckle pattern, leading to decreased confidence levels. Consequently, the *sigma* value holds significant promise for crack identification.

The calculation of the *sigma* value is dependent on the employed image correlation algorithm. As shown in Figure 17, the image correlation algorithm matches the subsets from the reference image as well as those correlated from the deformed image based on their pixel patterns (i.e., gray values of light intensity). Under the assumption of one-to-one correspondence, the ideal pixel pattern of $G\left(x + \bar{d}x, y + \bar{d}x\right)$ and $F(x,\ y)$ should be the same. Noises from image capture and the environment affect the light intensity pattern of the specimen surface in real applications. DIC employed an iterative numerical algorithm to find the matched subsets by minimizing the squared difference in pixel values, as shown in Equation 12 [37].

Figure 17. Matching process in DIC image analysis

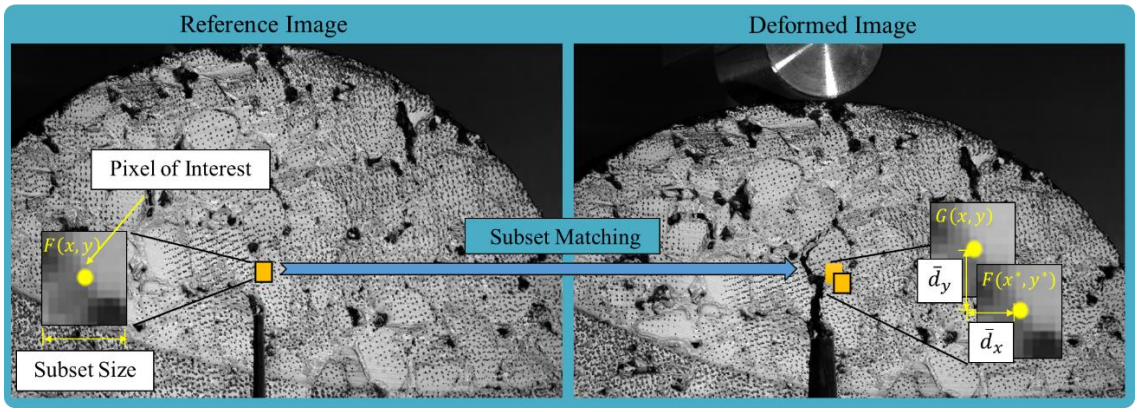

$$(\bar{d}_{x,\ opt}, \bar{d}_{y,opt}) = argmin \sum |G(x + \bar{d}x, y + \bar{d}x) - F(x,\ y)|^2 \qquad (12)$$

where,

G(x, y), F(x, y) = the light intensity value (gray-value) at pixel (x, y) from deformed image and reference image, respectively;

$\bar{d}x$, $\bar{d}y$ = current estimate of average displacements in x and y direction; and

$\bar{d}_{x,opt}$, $\bar{d}_{y,opt}$ = the optimal average displacements in x and y direction.

If the motion is sufficiently small, the gray values around a point of interest can be approximated by a first-order Taylor series expansion, as represented in Equation 13. In Equation 14, the pixel pattern *G* is expanded to *N* pixels with the subset, and it can be further transformed to Equation 15 to solve the displacement components *dx* and *dy*, known as the differential method [37]. This system of equations becomes overdetermined when the number of pixels in the subset exceeds two. Consequently, displacement components can be determined uniquely unless all gray-value derivatives are zero.

$$\frac{\partial G}{\partial x} dx = \Delta G \tag{13}$$

$$\begin{bmatrix} \frac{\partial G^1}{\partial x} & \frac{\partial G^1}{\partial y} \\ \frac{\partial G^2}{\partial x} & \frac{\partial G^2}{\partial y} \\ \vdots & \vdots \\ \frac{\partial G^n}{\partial x} & \frac{\partial G^n}{\partial y} \end{bmatrix} \begin{bmatrix} \bar{d}_x \\ \bar{d}_y \end{bmatrix} = - \begin{bmatrix} \Delta G^1 \\ \Delta G^2 \\ \vdots \\ \Delta G^n \end{bmatrix} \tag{14}$$

$$\begin{bmatrix} \bar{d}_x \\ \bar{d}_y \end{bmatrix} = - \begin{bmatrix} \sum \left(\frac{\partial G}{\partial x}\right)^2 & \sum \left(\frac{\partial G}{\partial x} \frac{\partial G}{\partial y}\right) \\ \sum \left(\frac{\partial G}{\partial x} \frac{\partial G}{\partial y}\right) & \sum \left(\frac{\partial G}{\partial y}\right)^2 \end{bmatrix}^{-1} \begin{bmatrix} \sum \left(\frac{\partial G}{\partial x}\right) \Delta G \\ \sum \left(\frac{\partial G}{\partial y}\right) \Delta G \end{bmatrix} \tag{15}$$

where,

n = the number of pixels of subset, which is the square of subset size; and

ΔG^i = the difference of light intensity value at i_{th} pixel.

In the differential method, two underlying assumptions have been made. First, the motion has to be sufficiently small for the first-order Taylor series expansion to be valid. Second, the motion has to be approximately constant throughout the neighborhood used for motion estimation. However, in real applications, those two assumptions are often broken. The iterative method, known as the Lucas-Kanade Tracker, is used as shown in Equations 16 and 17 [41]. The iterative algorithm searches for the p_{th} iteration, $\bar{d}^{p+1}$, until convergence to the optimal motion vector $\bar{d}_{opt}$.

$$\begin{bmatrix} \Delta\bar{x} \\ \Delta\bar{y} \end{bmatrix} = - \begin{bmatrix} \sum \left(\frac{\partial G}{\partial x}\right)^2 & \sum \left(\frac{\partial G}{\partial x} \frac{\partial G}{\partial y}\right) \\ \sum \left(\frac{\partial G}{\partial x} \frac{\partial G}{\partial y}\right) & \sum \left(\frac{\partial G}{\partial y}\right)^2 \end{bmatrix}^{-1} \begin{bmatrix} \sum \left(\frac{\partial G}{\partial x}\right) \Delta G \\ \sum \left(\frac{\partial G}{\partial y}\right) \Delta G \end{bmatrix} \tag{16}$$

$$\begin{bmatrix} \bar{d}_x^{p+1} \\ \bar{d}_y^{p+1} \end{bmatrix} = \begin{bmatrix} \bar{d}_x^{p} \\ \bar{d}_y^{p} \end{bmatrix} + \begin{bmatrix} \Delta\bar{x} \\ \Delta\bar{y} \end{bmatrix} \tag{17}$$

where,

$\bar{d}_x$ and $\bar{d}_y$ = the current estimates for the average motion of the subset; and

$\Delta\bar{x}$ and $\Delta\bar{y}$ = the incremental motion updates sought in the current iteration.

The optimal algorithms were used for the matching of subsets in DIC image analysis, which involves bias and errors. Additionally, bias and errors stem from the interpolation of pixel gray values. DIC utilizes an interpolation model for gray values to achieve measurements at sub-pixel resolution. In practical testing, the DIC images are always contaminated by some noise, which could come from image capture and changes in the environmental lighting conditions. To estimate the effects of noise, a confidence margin value (i.e., *sigma*) is reported for each output data point from the VIC-3D software. A higher *sigma* value indicates there is more noise between the reference image and the deformed image, resulting in lower confidence for the matched results.

The *sigma* value has the potential to evaluate the cracking extent and identify the cracked area during the cyclic SCB test. During the fatigue test, the cracks propagated from micro-cracks to macro-cracks. The crack propagation introduced large-scale deformations and damaged the speckle patterns, which introduced noise in the matching process of DIC image analysis. For two-dimensional measurements, the covariance matrix can be approximated as shown in Equation 18 [37]. The *sigma* value is reported in common commercial DIC software, such as VIC-3D [36].

$$Var(\bar{t}) = \frac{1}{N}|G-F|^2 \begin{bmatrix} \sum\left(\frac{\partial F}{\partial x}\right)^2 & \sum\left(\frac{\partial F}{\partial x}\frac{\partial F}{\partial y}\right) \\ \sum\left(\frac{\partial F}{\partial x}\frac{\partial F}{\partial y}\right) & \sum\left(\frac{\partial F}{\partial y}\right)^2 \end{bmatrix}^{-1} = \frac{1}{N}|G-F|^2\boldsymbol{H} \quad (18)$$

Figure 18 shows an example of a *sigma* color map surrounding the crack tip during the cyclic SCB test. Across the specimen surface, the majority of *sigma* with lower values (i.e., approximately less than 0.02, colored blue and green) are related to the non-cracked area, representing a low level of error resulting from the noise in image capture or environmental effects. Conversely, the *sigma* distribution clearly showed a positive correlation between higher *sigma* values and increased cracking area, likely due to additional errors caused by the damaged speckle pattern. For areas that have fully cracked, the *sigma* value is not applicable because the matching process was unsuccessful. Therefore, the confidence margin (i.e., *sigma*) could have great potential for the identification of cracking. Higher *sigma* values are associated with areas with excessive cracking.

Figure 18. Matching process in DIC image analysis

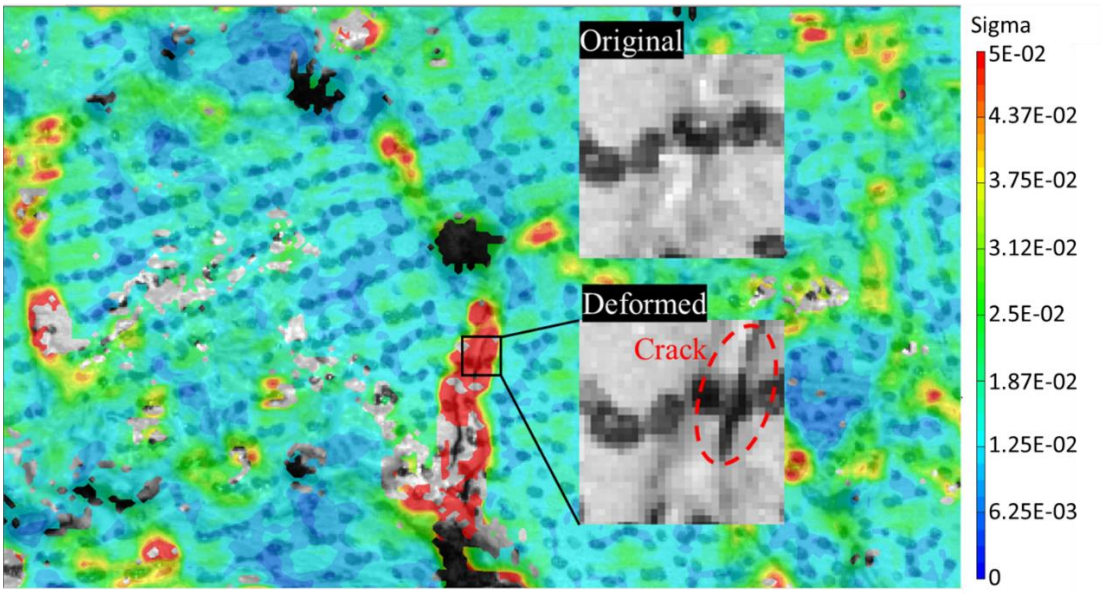

Statistical Analysis of Confidence Margins

Given the significant potential of the confidence margin (i.e., *sigma*) in crack identification during the cyclic SCB test, a statistical analysis-based approach was developed to establish the *sigma* criteria, which was then used to measure crack lengths. As stated previously, the *sigma* value was calculated from the speckle pattern gradient and the difference between matched subsets. When considering all data points from an undeformed image with a given speckle pattern, the *sigma* values associated with these points should be independent of the subset size and should follow a specific statistical distribution. This distribution can be referred to as an undeformed distribution. Based on the aforementioned assumptions, the following hypothesis can be formulated:

1. **Null Hypothesis H0:** The *sigma* value of a given subset follows the undeformed distribution.
2. **Alternative Hypothesis H1:** The *sigma* value of a given subset does not follow the undeformed distribution, indicating the potential influence of other factors, such as cracking.

Figure 19 shows an example of a *sigma* frequency count from an undeformed image. It was found that the undeformed distribution of *sigma* can be approximated by the inverse Gaussian distribution. In Equation 18, the estimation of the covariance matrix is calculated

by dividing the matching error ($\frac{1}{N}|G - F|^2$) by the Hessian matrix, H. The numerator matching error represents the difference in pixel values between the matched subsets, and the divisor Hessian matrix represents the speckle pattern gradient. In real-world applications, analysis of the undeformed image revealed that the matching error is negligible compared to its divisor, and the Hessian matrix follows the Gaussian distribution. Consequently, the *sigma* distribution can be approximated as an inverse Gaussian distribution. This approximation is verified by fitting the observed data to an inverse Gaussian statistical model.

Figure 19. Example of *sigma* frequency count from undeformed image

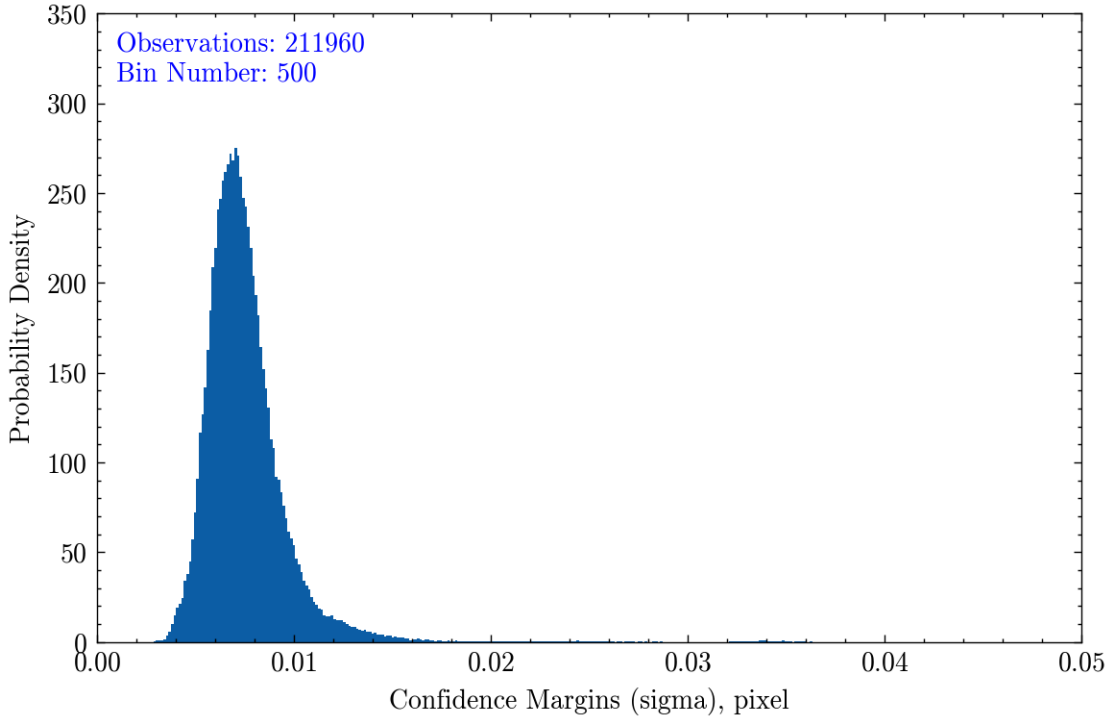

The probability density function (PDF) of an inverse Gaussian model was used to fit the *sigma* distribution data. The PDF is a fundamental concept in probability theory and statistics used for describing the likelihood of a continuous random variable taking on a specific value [42]. The integral of the PDF over a particular interval gives the probability that the random variable falls within that interval; see Equation 19. For discrete *sigma* values, the PDF can be calculated from histogram data; see Equation 20 [42].

$$Pr(a < x \leq b) = \int_a^b f(x)dx \tag{19}$$

where,
$Pr(x)$ = probability of random variable; and
$f(x)$ = probability density function of random variable.

$$f(x_i) = Pr(x_i - \frac{dx}{2} < x \leq x_i + \frac{dx}{2})/dx = \frac{n_i}{N \cdot w_i} \quad (20)$$

where,
n_i = frequency of i_{th} bin;
N = total number of observations; and
w_i = width of i_{th} bin.

Figure 20 shows an example of *sigma* distribution data fitted to an inverse Gaussian distribution model. Equation 21 gives the PDF of the inverse Gaussian distribution model, and the mean squared error (MSE) values are calculated to evaluate the goodness of the fit in Equation 22. The *sigma* data was found to have a good fit with the inverse Gaussian distribution model.

It is noted that the *sigma* values report data points from an undeformed image (i.e., no loading is applied). Since no load was applied, the *sigma* values were exclusively controlled by the speckle patterns and matching errors.

$$IG(x) = \sqrt{\frac{\lambda}{2\pi x^3}} \cdot e^{-\frac{\lambda(x-\mu)^2}{2\mu^2 x}} \quad (21)$$

where,
$IG(x)$ = probability density function of the inversed Gaussian model, x = random variable;
μ = mean of the distribution; and
λ = shape parameter of the distribution.

$$MSE = \frac{1}{n}\sum_{i=1}^{n}(y_i - \hat{y}_i)^2 \quad (22)$$

where,
MSE = mean squared error;
n = the number of data points;
y_i = the observed value; and
$\hat{y}_i$ = the predicted value.

Figure 20. Statistical model fitting and criteria determination of *sigma*

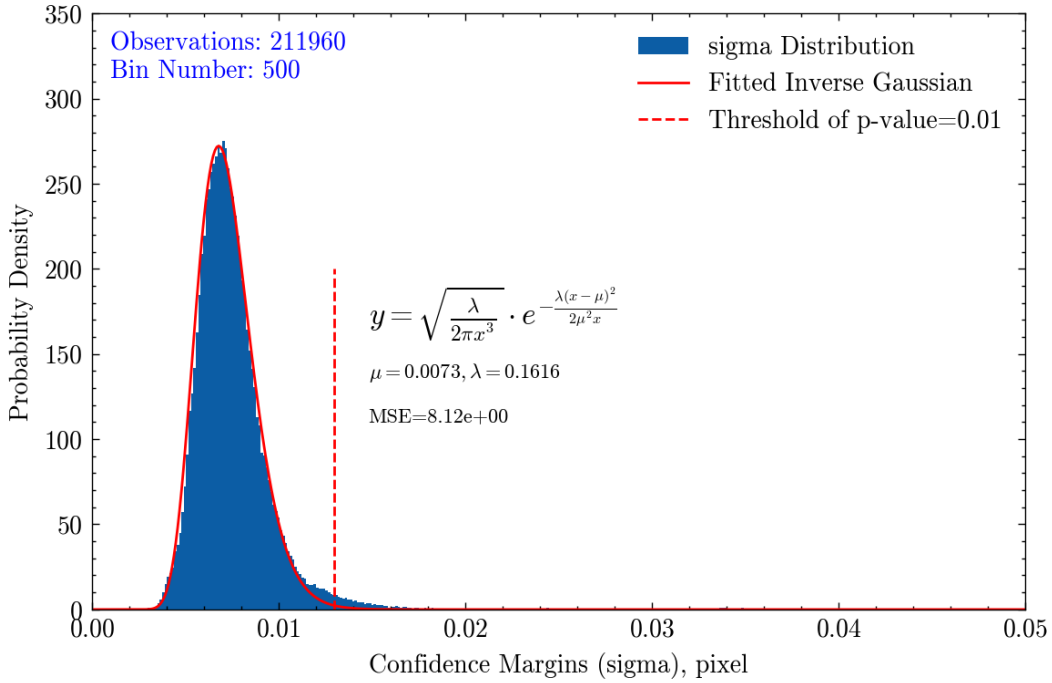

The *sigma* criterion was determined according to the fitted statistical model. The *sigma* value with a p-value of 1% (i.e., $sigma_{0.01}$) was selected as the criteria for rejecting the null hypothesis. A *sigma* greater than $sigma_{0.01}$ for a subset indicates that there is less than a 1% probability of the null hypothesis being true. Consequently, the alternative hypothesis is true, suggesting that the subset is affected by cracking. The $sigma_{0.01}$ can be determined by integrating the probability density function (PDF) until the cumulative probability in the right tail equals 1%.

Crack Length Identification Based on Confidence Margins

The *sigma* criterion determined from the undeformed image was applied to each frame for Fracture Process Zone (FPZ) identification throughout the cyclic SCB test. The FPZ were determined as the areas with *sigma* values greater than $sigma_{0.01}$. In Figure 18, the FPZ around cracks was successfully identified. However, there were other small areas that were also marked as FPZ due to voids or poor patterns, which were not related to crack propagation. In order to identify the crack length in the FPZ areas, a technique was developed to recognize the crack-related FPZ. The crack-related FPZ was further used for crack length identification.

The crack length identification process consists of three steps. First, the Connected Component Analysis (CCA) was used to group connected areas [43]. CCA is a widely used technique in image processing for detecting and labeling clusters of connected pixels within a binary image. In practice, CCA involves scanning the binary image to group adjacent pixels that share the same binary value. Each group, or connected component, was then assigned a unique label, enabling the differentiation of individual objects within the image; see Figure 21. Each group represents a continuous area of FPZ. Further, the group that contains the notch tip was selected from all labeled groups. The area originating from the notch tip can be identified as the crack-related FPZ. Finally, the crack length was determined as the vertical distance between the crack tip and the notch tip. It is noted that the measured crack length does not include notch depth. A Python script was developed to process the analysis for crack length identification.

Figure 21. Illustration of Connected Component Analysis (CCA) in binary image

0	0	0	0	0	0	0	0	0	0	0	0	0	0
0	1	1	0	0	0	0	0	3	3	3	3	0	0
0	1	1	1	0	0	0	0	3	3	3	3	0	0
0	1	1	1	0	0	0	0	0	3	3	3	0	0
0	0	0	0	0	0	0	0	0	0	0	0	0	0
0	0	0	2	2	2	2	2	2	0	0	0	0	0
0	0	0	2	2	2	2	2	2	0	0	0	0	0
0	0	0	2	2	2	2	0	0	0	0	0	0	0
0	0	0	0	0	0	0	0	0	0	0	0	0	0

Figure 22 illustrates the CCA and crack length measurement processes. The crack-related FPZ and other areas were initially filtered out by implementing the $sigma_{0.01}$threshold, which is marked as red in subplot *a*. After conducting the CCA, the groups of continuous areas were assigned different labels, which are marked as different colors in subplot *b*. Subplot *c* illustrates the recognition of crack-related FPZ and the calculation of crack length.

Figure 22. Crack length identification

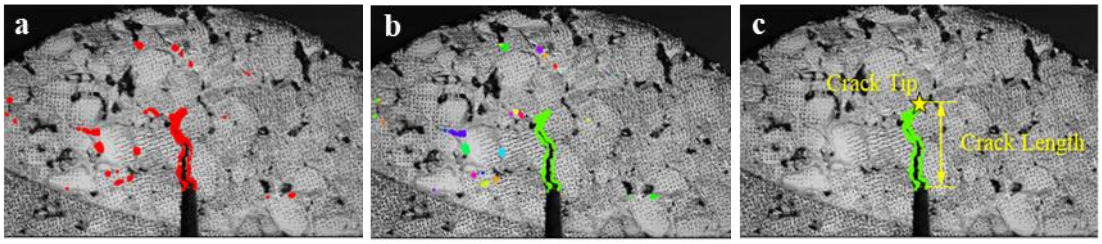

(a) FPZ areas **(b) Connected Component Analysis** **(c) Cracked related FPZ**

Applying the developed method to each frame of the cyclic SCB test allows for FPZ and crack length identification, resulting in a crack length curve used for the Paris' Law modeling. Figure 23 shows an example of the FPZ identification process, along with its corresponding *sigma* distribution across different load cycles. As crack propagation progressed, the number of identified FPZs increased, accompanied by rising *sigma* values above the threshold. Therefore, this method could effectively be used to identify the crack length for each frame.

Figure 23. Illustration of FPZ identification and associated *sigma* distribution

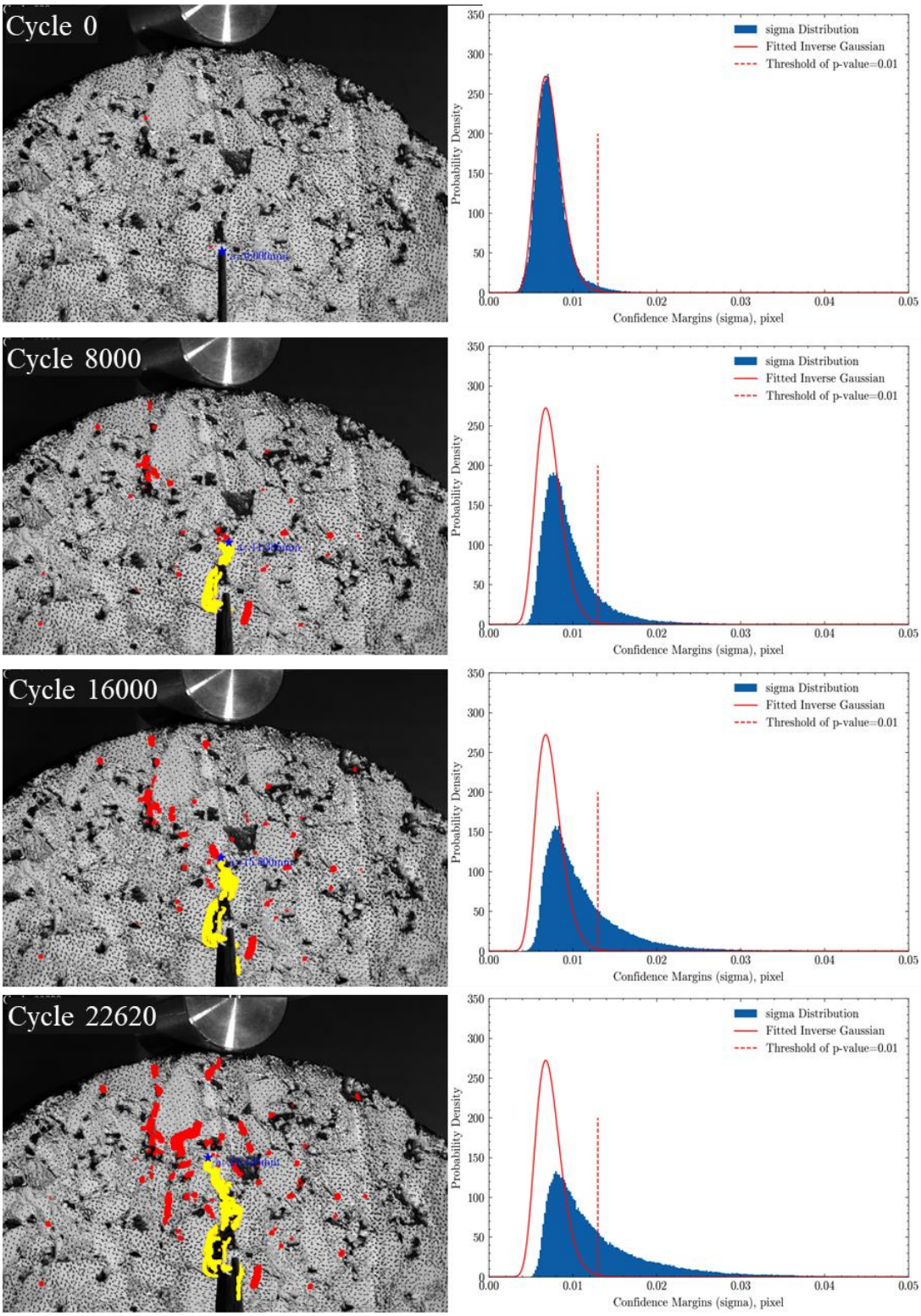

Figure 24 presents the identified crack length curve for one sample. Due to the spatial resolution of the DIC results and the influence of large aggregates and voids, the raw data points of the crack length curve appear to be step-shaped. To smooth the crack length curve, a sigmoid function was employed. The smoothing of the crack length curve is necessary to generate a consistent and accurate crack propagation rate, and further facilitate a more precise Paris' Law analysis. Equation 23 shows the sigmoid function for smoothing the crack length curve. Correlating crack length with normalized load-line displacement (i.e., LLD_{norm}) rather than load cycle number provides a better fit for smoothing the curve. Therefore, a scatter plot of LLD_{norm} versus crack length was used to smooth the curve. The LLD curve was obtained from the integrated sensor of the MTS device during the cyclic SCB test and correlated with the crack length data points based on cycle number. The normalized load-line displacement LLD_{norm} was calculated by dividing the LLD values by the maximum LLD. Figure 24 also shows the LLD versus crack length curve and its smoothed version.

Figure 24. Crack length curve for cyclic SCB test

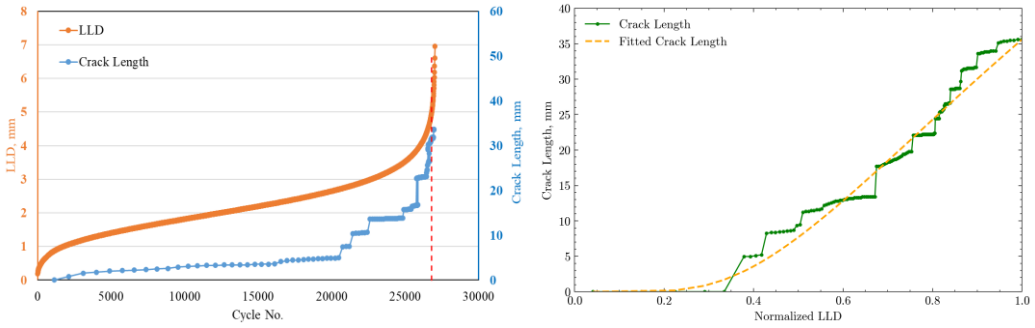

(a) Crack length and LLD vs. load cycle number **(b) Crack length vs. LLD_{norm} and curve smoothing**

$$a = L * e^{k\left(1-\frac{1}{LLD_{norm}}\right)} \quad (23)$$

where,

a = crack length, mm;

LLD_{norm} = the normalized LLD, which = calculated by dividing LLD by the maximum LLD, ranges from 0 to 1; and

L and k = shape coefficients.

Prediction Model of Asphalt Pavement Fatigue Life Based on Paris' Law

This section first discusses the application of a fatigue model based on the Paris' Law coefficients that measured from the developed cyclic SCB test. The model's prediction

results were compared to those obtained from the Pavement ME model. The fatigue model inputs include material properties and pavement mechanistic responses. The pavement responses were analyzed based on finite element (FE) modeling of the pavement structure. Four pavement structures with varying asphalt layer thickness and three mixtures (i.e., 76R0, 70R30, and 67R50) with different fatigue cracking resistance were used to predict the fatigue life. The viscoelastic properties of mixtures were characterized by the dynamic modulus test.

Second, a modified Pavement ME model was preliminarily developed for improved prediction of pavement fatigue life. Two mixtures were evaluated by the developed cyclic SCB test, and the measured Paris' Law coefficients were introduced to the Pavement ME model as part of the inputs. The developed model was preliminarily calibrated, and its prediction results were compared to the original Pavement ME model.

Dynamic Modulus Test

Dynamic modulus tests were conducted for the three mixtures: 76R0, 70R30, and 67R50. Cylindrical specimens were subjected to frequency sweep loading at multiple temperatures. For each mixture, three specimens were compacted using a Superpave gyratory compactor (SGC) to a height of 170 mm and a diameter of 150 mm. The samples were then cored and trimmed to obtain test specimens with a dimension of 150 mm in height and 100 mm in diameter. The target air-void content for test specimens was 7.0±0.5%. All test specimens were subjected to oven aging at 85°C for 120 hours in accordance with AASHTO R30 prior to testing [40]. The dynamic modulus tests were conducted in accordance with the AASHTO TP62-10 testing protocol [44] using the asphalt mixture performance tester (AMPT). The tests were conducted at four temperature levels (i.e., 4.4, 25, 37, and 54°C) and at six loading frequencies (i.e., 25, 10, 5, 1, 0.5, and 0.1 Hz) for each of the four temperatures.

Pavement Mechanistic-Empirical (ME) Model

Traditionally, fatigue cracks in asphalt pavements have been attributed to tensile strains generated at the bottom of the asphalt layer due to repeated traffic loading. The fatigue damage initiates at the bottom as micro-cracks. These micro-cracks propagate upward and eventually develop into visible cracks on the surface as longitudinal or transverse cracks in wheel paths. Since crack initiation and propagation involve very complex mechanisms at multi-scales and different fracture modes, translating from controlled laboratory fatigue testing to field fatigue prediction is difficult.

The Pavement ME Design utilizes a mechanistic-empirical model to predict the allowable number of load repetitions for a given tensile strain at the bottom of the asphalt layer, as detailed in Equations 24 to 26 [45]. The inputs of this model include pavement structure thickness, asphalt layer tensile strain, and the mixture's dynamic modulus and volumetric properties.

To predict fatigue life, the dynamic modulus |E*| in Equation 24 was determined by interpolating the dynamic modulus master curves at a reference temperature of 20°C and a loading frequency of 2.5 Hz. The model coefficients for the Pavement ME fatigue model are presented in Table 4. These coefficients have been sourced from the latest updates available on the official website [45].

$$N_f = 0.00432 * C * \beta_{f1} k_1 (\frac{1}{\varepsilon_t})^{k_2 \beta_{f2}} (\frac{1}{|E^*|})^{k_3 \beta_{f3}} \quad (24)$$

$$C = 10^{4.84(\frac{V_{be}}{V_a + V_{be}} - 0.69)} \quad (25)$$

$$\beta_{f1} = 5.014 * (H_{AC})^{-3.416} \quad (26)$$

where,
N_f = allowable number of load repetitions to fatigue cracking;
ε_t = tensile strain at the bottom of asphalt layers;
$|E^*|$ = dynamic modulus of the asphalt mixture, MPa;
C_H = thickness correction in terms for fatigue cracking;
$k_{1\text{-}3}$ = regression coefficients;
V_{be} = effective binder content by volume, %;
V_a = air void content, %; and
H_{AC} = total thickness of asphalt layers, in.

Table 4. Pavement ME fatigue model coefficients

Pavement ME Fatigue Model Coefficient	Coefficient Value
k1	3.75
k2	2.87
k3	1.46
β2	1.38
β3	0.88

Pavement Fatigue Life Model Based on Paris' Law Equation

The Paris' Law model is a mechanistic approach based on fracture mechanics for fatigue life prediction. Paris' Law relates the rate of fatigue crack growth to the range of the stress intensity factor *ΔK*. In the Paris' Law model (see Equations 7 to 8), the fatigue life of pavements can be predicted by integrating the crack propagation rate in terms of load cycle numbers, as shown in Equation 27. The Paris' Law coefficients *n* and *Log(A)* represent fundamental material properties of AC that are obtained from the cyclic SCB test.

$$N_f = \int_{a_0}^{H} \frac{da}{A(\Delta K)^n} \quad (27)$$

where,
N_f = fatigue life;
a_0 = Initial crack length, mm; and
H = Asphalt layer thickness, mm.

The stress intensity factor, *K*, is a critical parameter in fracture mechanics that represents the stress state near the tip of a crack. The calculation of *ΔK* for an asphalt layer involves understanding the response of the material pavement structure to the applied traffic loading. The stress state of the AC layer under traffic loading can be approximated as that of a bending beam or plate [9, 35]. Consequently, crack propagation within the AC layer can be modeled using an edge-cracked plate under plane strain conditions. Equations 28 and 29 provide the calculation for *ΔK* in this specific case. Similar to Equation **Error! Reference source not found.** for Paris' Law fitting, the ΔK can be replaced with the stress intensity factor, K_I, at the maximum load within a cycle. A geometric factor is multiplied in the ΔK calculation to reflect stress localization at the crack tip, which is a function of the crack-thickness ratio.

$$K_I = f\left(\frac{a}{H}\right)\sigma\sqrt{\pi a} \quad (28)$$

$$f\left(\frac{a}{H}\right) = \frac{6\sqrt{2\tan\left(\frac{\pi}{2H}\right)}}{\cos\left(\frac{\pi}{2H}\right)}\left\{0.923 + 0.199\left[1 - \sin\left(\frac{\pi a}{2H}\right)\right]^4\right\} \quad (29)$$

where,

K_I = stress intensity factor, kN·m$^{-1.5}$;

$f\left(\frac{a}{H}\right)$ = Geometric factor; a - crack length, mm;

σ = maximum tensile stress, kPa; and

H = Asphalt layer thickness, mm.

In this study, the pavement mechanical responses were simulated by finite element (FE) analysis. The FlexPAVE software was used for finite element modeling of asphalt pavement [46]. The FE simulation incorporates the viscoelastic characteristics of asphalt, load distribution, and temperature effects to model asphalt pavement structure. By simulating the pavement mechanical response, the critical tensile strain and tensile stress at the bottom of the asphalt layer were determined and used as inputs for the Pavement ME and Paris' Law fatigue models. To account for the effects of asphalt layer thickness on pavement responses, four pavement structures were analyzed: 2, 4, 6, and 8-in. asphalt layers. The detailed finite element (FE) model for asphalt pavement is provided in Appendix A.

Development of Modified Pavement ME Model

The material inputs of the Pavement ME model rely on volumetric properties and the dynamic modulus. However, these inputs are inadequate to characterize the fatigue cracking performance of mixtures, especially considering the growing use of unconventional materials such as RAP and crumb rubber in asphalt mixtures. When modeling these materials in Pavement ME, using default fatigue material parameters does not accurately predict observed field performance, as reported by other researchers [47, 48]. In this section, the Paris' Law coefficients obtained from the developed cyclic SCB test were introduced in the Pavement ME model for improved prediction of pavement fatigue life. Two mixtures obtained from were evaluated by the developed cyclic SCB test and its results were used for preliminary calibration of the modified Pavement ME model.

Equation 30 presents the modified Pavement ME model, where the calculation for coefficients C and β_{f1} are the same as Equation 25 and Equation 26, respectively. The modified Pavement ME model incorporates the cracking propagation characteristics of

asphalt mixture to improve the prediction of pavement fatigue life. It is noted that the absolute value of *Log(A)* is used to ensure the regression coefficient β_{f4} positive. The inputs of coefficients are the same as in Table 4, except the added coefficients C_2, β_{f4}, and β_{f5}.

$$N_f = 0.00432 * C * \beta_{f1} k_1 \left(\frac{1}{\varepsilon_t}\right)^{k_2\beta_{f2}} \left(\frac{1}{|E^*|}\right)^{k_3\beta_{f3}} * C_2 * (|Log(A)|)^{\beta_{f4}} (\frac{1}{n})^{\beta_{f5}} \quad (30)$$

where,
N_f = allowable number of load repetitions to fatigue cracking;
ε_t = tensile strain at the bottom of asphalt layers;
$|E^*|$ = dynamic modulus of the asphalt mixture, MPa;
C_H = thickness correction in term for fatigue cracking;
$k_{1\text{-}3}$ = regression coefficients;
V_{be} = effective binder content by volume, %;
V_a = air-void content, %;
H_{AC} = total thickness of asphalt layers, in.;
C_2, β_{f4}, β_{f5} = regression coefficients; and
Log(A), n = Paris' Law coefficients.

Two asphalt mixtures were obtained from a full-scale test at the Federal Highway Administration (FHWA) Accelerated Loading Facility (ALF) that have RAP contents, designated as L8 and L11 [49]. The warm mix technique Evotherm was used for mixture L11. Both mixtures contain 40% RAP in terms of recycled binder ratio (RBR), which is defined as the percentage of recycled asphalt in the total asphalt binder of the mixture [49]. The asphalt loose mixtures of the ALF mixtures were acquired and transported to LTRC for laboratory characterization. Table 5 presents the asphalt mixture composition properties for the ALF mixtures.

The two ALF mixtures were evaluated by the developed cyclic SCB test and the measured Paris' Law coefficients were used in preliminary calibration of the modified Pavement ME model. The field performance fatigue life measured from the ALF test is used in comparative analysis with the predicted fatigue life by the prediction model. The measured fatigue lives from ALF were determined as the number of load passes to the first appearance of surface cracking [50].

Table 5. Asphalt mixture composition for ALF mixtures

Mix Designation	Air Void (%)	VMA (%)	Asphalt Content (%)	RAP RBR (%)	Virgin Binder PG	HMA/WMA Process
L8	4.9	16.4	4.95	40	58-28	HMA
L11	4.9	16.5	4.89	40	58-28	Evotherm

Discussion of Results

Optimization of Testing Parameters of Cyclic SCB Test

Factorial Design Results of Cyclic SCB Test

Table 6 presents the cyclic SCB results of the full factorial design, including the number of cycles to failure N_f and Paris' Law coefficients, *Log(A)* and *n*. A total of nine groups of different combinations of testing parameters were conducted, which were denoted as notch depth + loading frequency. The average and coefficient of variance (CoV) values were computed from four replicate samples for each group. The CoV of N_f ranges from 11.3% to 24.9%, whereas relatively lower CoV results were observed for the Paris' Law coefficients. The CoV of *n* ranged from 8.1% to 17.1%, whereas that of *Log(A)* ranged from 7.5% to 13.3%. The CoV values indicate that the cyclic SCB test exhibits good repeatability.

Table 6. Cyclic SCB results at different combinations of testing parameters

Factorial Group	Average			Coefficient of Variance		
	N_f	*n*	*Log(A)*	N_f	*n*	*Log(A)*
15mm+1Hz	9884	4.222	-12.352	24.9	17.1	13.3
20mm+1Hz	5210	4.689	-13.428	20.5	13.9	11.5
25mm+1Hz	2347	4.877	-13.784	20.8	16.1	10.0
15mm+5Hz	36182	4.137	-14.452	21.7	13.5	10.5
20mm+5Hz	27293	4.438	-15.661	14.3	11.1	6.8
25mm+5Hz	16295	4.356	-15.757	18.3	15.7	9.0
15mm+10Hz	147156	3.577	-16.017	22.6	12.5	9.2
20mm+10Hz	55094	3.917	-16.422	11.3	8.1	7.5
25mm+10Hz	25645	3.726	-16.730	15.2	9.4	9.7

Effects of Testing Parameters on Cyclic SCB Test

Figure 25 shows the effects of different testing parameters on the measured performance indicators N_f and Paris' Law coefficients. The results for the nine groups of tests were sorted

in two ways to investigate the individual effects of notch depth and loading frequency. A one-way analysis of variance (ANOVA) was conducted to determine if there were significant differences in results across different levels of the testing parameters. To identify specific differences among groups, a post hoc Duncan's test was performed at a 0.05 significance level [51]. The results of the ANOVA analysis were presented using letter groupings. Different letters indicate statistically significant differences between groups.

As shown in Figure 25, both loading frequency and notch depth significantly influenced the number of cycles to failure, N_f. It was observed that N_f decreased with increasing notch depth and loading frequency. An increase in loading frequency resulted in higher strength in the AC material due to the asphalt binder's viscoelasticity (i.e., shear thickening). Conversely, a higher notch depth resulted in an increased concentration of tensile stresses at the notch tip. The observed effects of loading frequency and notch depth on N_f were consistent with the theoretical analysis. The statistical results also indicate that groups with different notch depths or loading frequencies exhibited significantly different N_f values. This observation implies that the N_f values obtained from the cyclic SCB tests are dependent on sample notch depth and loading frequency.

Figure 25. Effects of testing parameters on N_f

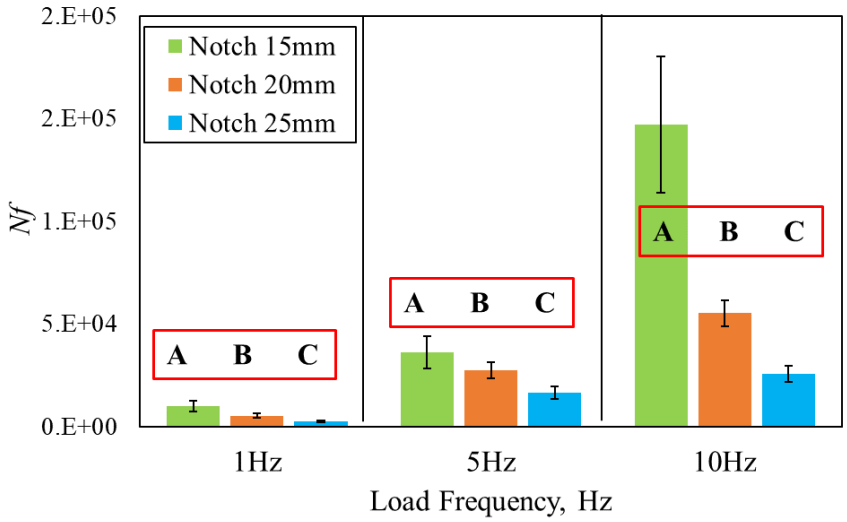

(a) Group by load frequency

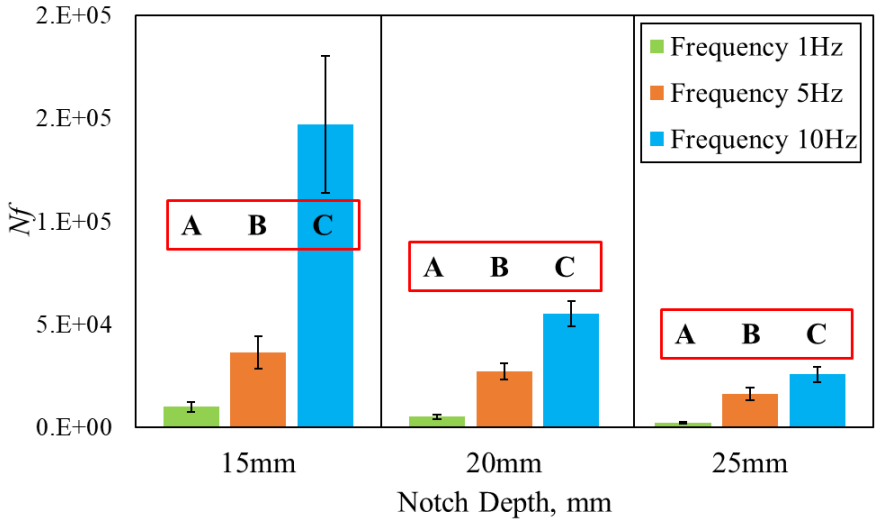

(b) Group by notch depth

Figure 26 and Figure 27 show the effects of testing parameters on the Paris' law coefficient values, *n* and *Log(A)*, respectively. Unlike the number of cycles to failure, N_f, the Paris' Law coefficients showed minimal variance between groups that used different combinations of sample notch depths and loading frequencies. The ANOVA groupings did not show any significant differences across groups of three different notch depths and loading frequencies. The Paris' Law coefficient values are independent of sample notch depth or loading frequency, indicating that they are fundamental material properties critical for crack resistance modeling [49].

Figure 26. Effects of testing parameters on Paris' Law coefficient *n*

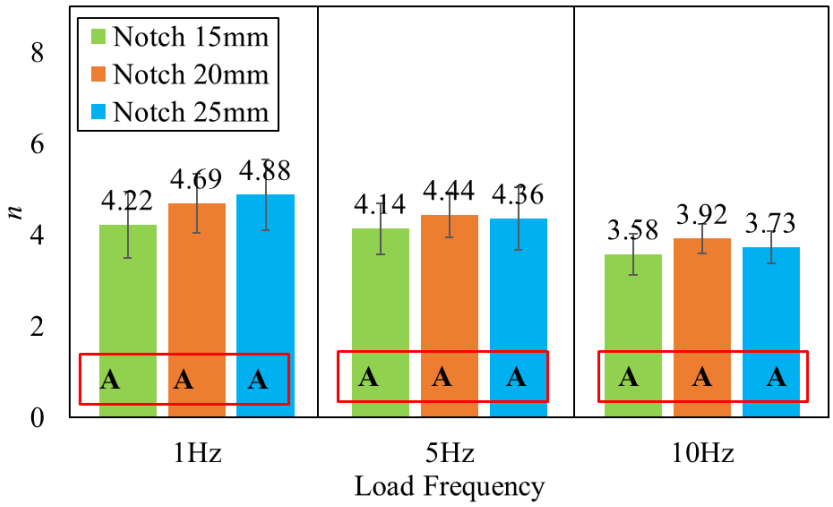

(a) Group by load frequency

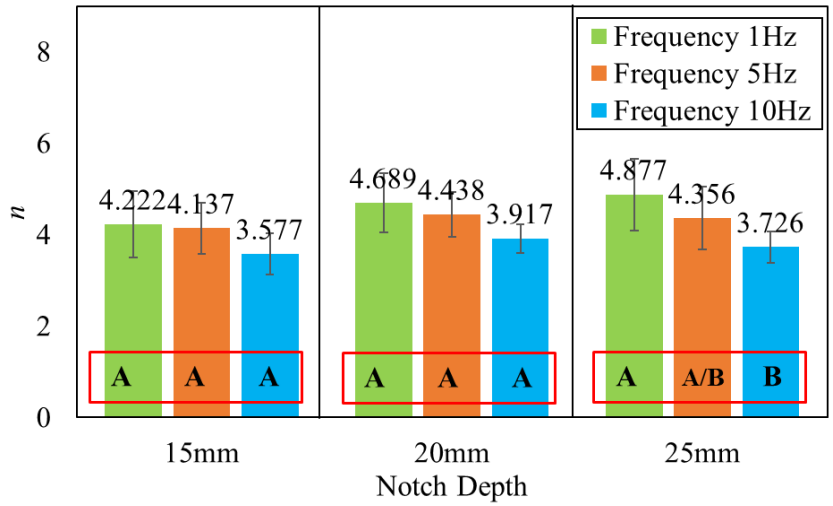

(b) Group by notch depth

Figure 27. Effects of testing parameters on Paris' Law coefficient *Log(A)*

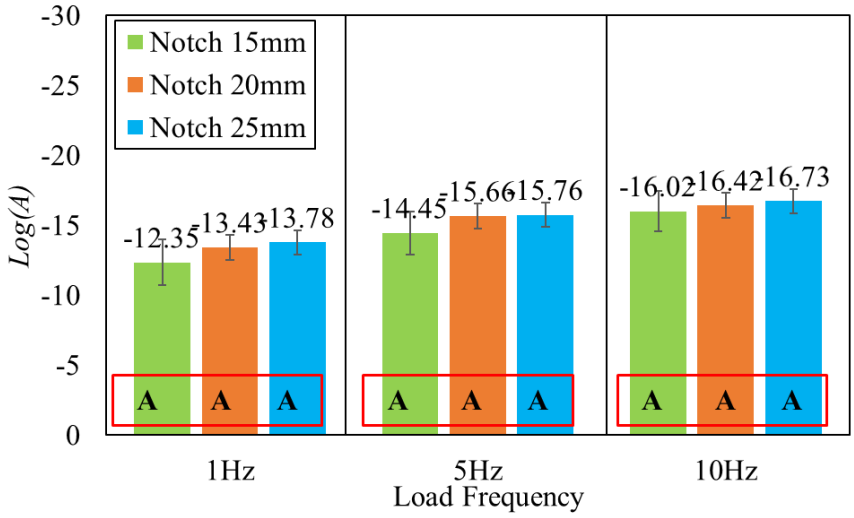

(a) Group by load frequency

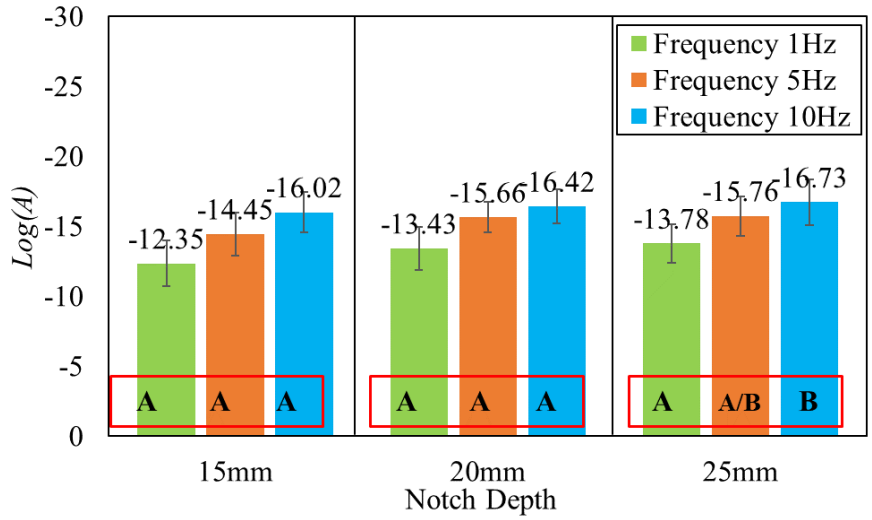

(b) Group by notch depth

Selection of Optimized Testing Parameters for Cyclic SCB Test

The optimized combination of testing parameters for the cyclic SCB test was selected according to test variance and practicality. Figure 28 presents the effects of loading frequency and sample notch depth on test variance, respectively. Each data point in Figure 28 represents the mean CoV values for all groups with the same factor level. For example, the mean CoV of 22.1% for a loading frequency of 1 Hz was averaged using data from groups 15mm+1Hz, 20mm+1Hz, and 25mm+1Hz. The CoV values decreased as the loading frequency increased.

Further, specimens with a notch depth of 20 mm showed lower CoV values at the same frequency level; see Figure 28b. It was found that the 20mm+10Hz combination yielded the lowest test variance for the Paris' Law coefficients. The 25mm+10Hz combination exhibited the second lowest variance for the indicators of the Paris' Law coefficients. The CoV values of the Paris' Law coefficients for these two combinations were found to be lower than 10%. However, it is essential to consider the practicality of selecting testing parameters. For a loading frequency of 10 Hz, samples with a notch depth of 20 mm required approximately twice the testing time compared to samples with a notch depth of 25 mm. To balance test repeatability and practicality, the combination of 25 mm notch depth and 10 Hz loading frequency was proposed as the optimized testing parameter for the cyclic SCB test.

Figure 28. Effects of testing parameters on variance of cyclic SCB results

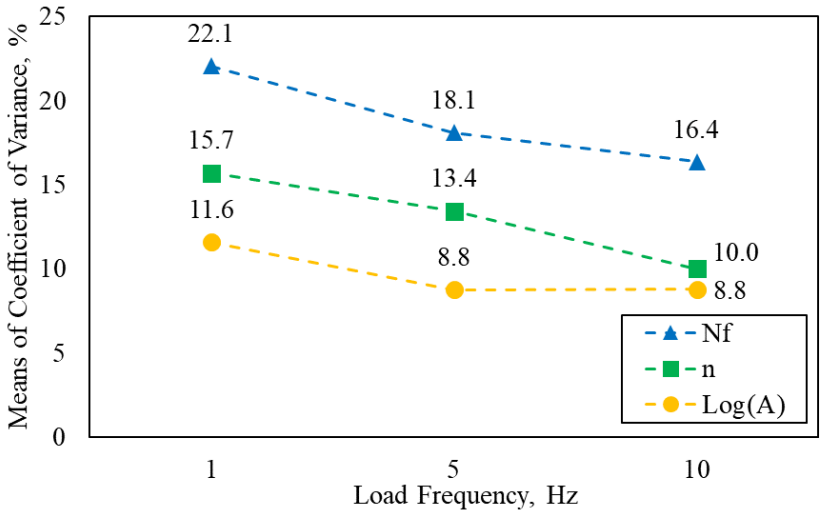

(a) Effects of load frequency

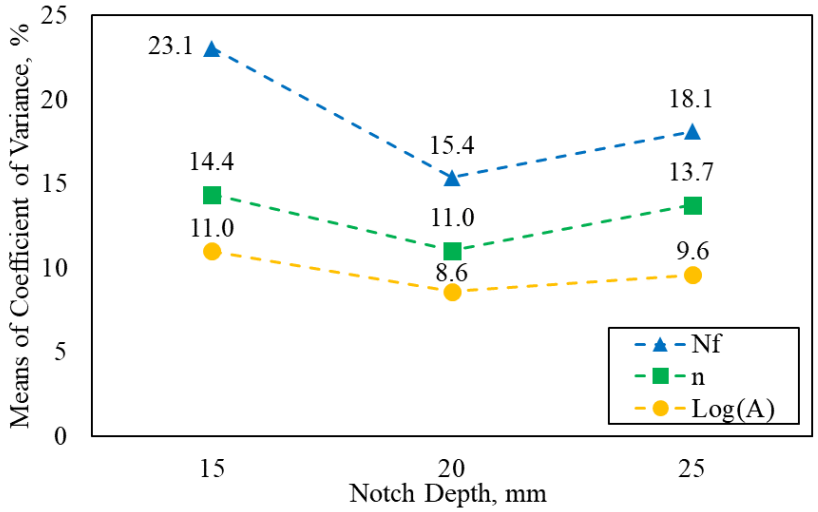

(b) Effects of notch depth

Sensitivity Analysis for Proposed Cyclic SCB Test Protocol

SCB-J_c Test Results

The standard SCB tests were conducted according to ASTM D8044 [1], and the critical strain energy release rate values, J_c, were computed for sensitivity analysis. Figure 29 shows the J_c values for the three mixtures considered for the sensitivity analysis. The J_c values decrease with decreasing cracking resistance of the mixtures; J_c values ranged from 0.98 for mixture 76R0 to 0.24 for mixture 67R50, reflecting the anticipated ranking of their cracking resistance.

Figure 29. SCB-J_c results for sensitivity analysis mixtures

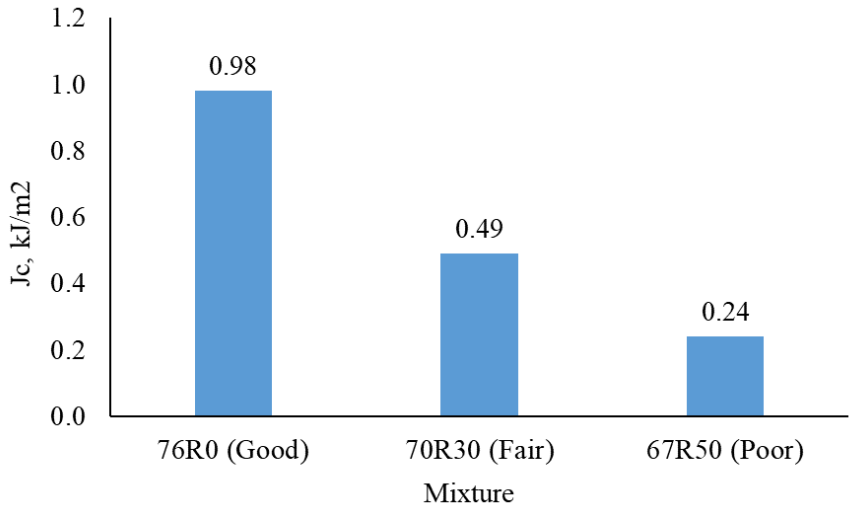

Discussion of Sensitivity Analysis Results

The proposed cyclic SCB test protocol was used to evaluate the mixtures 76R0, 70R30, and 67R50 for sensitivity analysis. The test results were expected to clearly exhibit different fatigue cracking resistances. The expected ranking of fatigue cracking resistance was 76R0 > 70R30 > 67R50. In the cyclic SCB test, optimized testing parameters were employed to evaluate the asphalt mixtures considered: 25 mm of notch depth and 10 Hz loading frequency. Figure 30 shows the Paris' Law fitting for the results of each mixture. Table 6 shows a summary of the two test parameters evaluated in the study: J_c and N_f.

Figure 30. Results of Paris' Law fitting for different mixtures

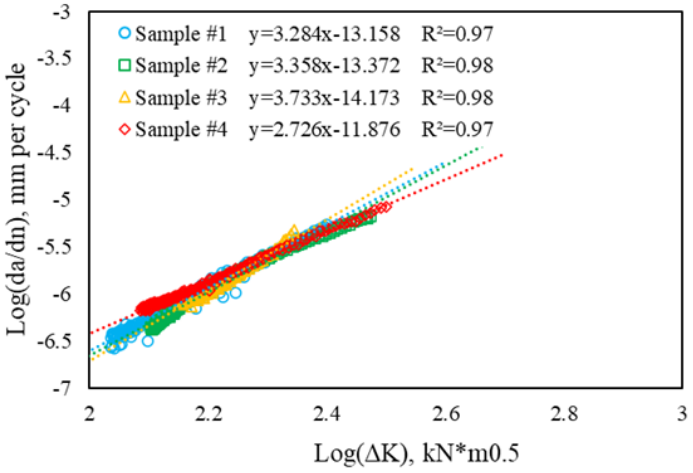

(a) Mixture 76R0

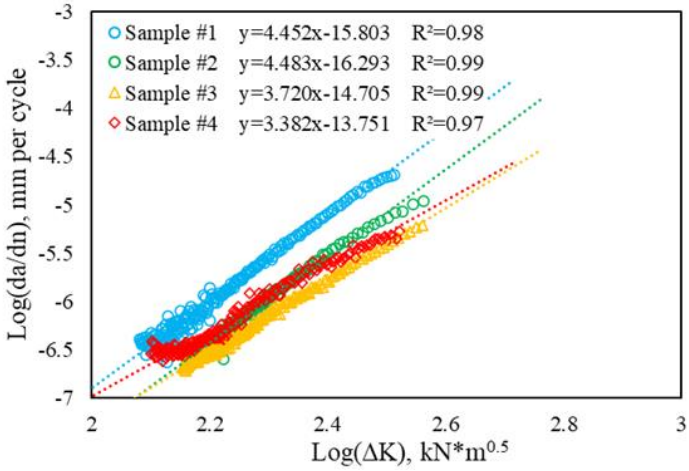

(b) Mixture 70R30

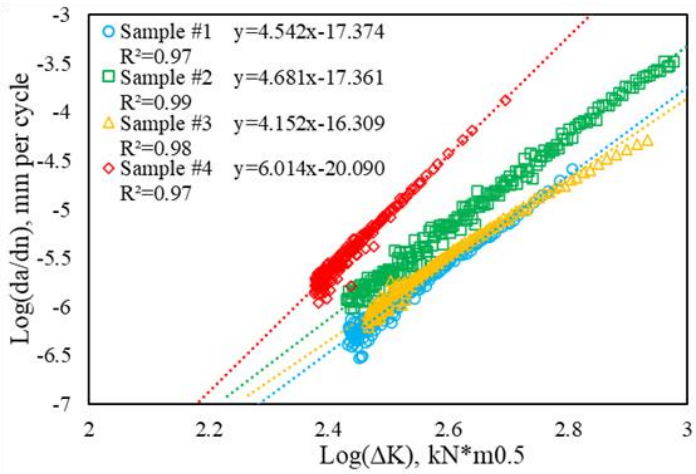

(c) Mixture 67R50

The average SCB strengths (i.e., peak load) obtained from the monotonic SCB were 1.03, 1.11, and 2.238 kN for mixtures 76R0, 70R30, and 67R50, respectively. Mixtures 76R0, 70R30, and 67R50 had SCB J_c values of 0.98, 0.49, and 0.24 kJ/m^2, respectively. It is noted that the SCB test was able to correctly rank these mixtures according to their expected crack resistance performance (i.e., mixtures with higher RAP/unmodified binder have lower crack resistance than those with lower RAP content/polymer modified mixtures). As seen in Table 7, the highest N_f value for observed for 70R30, followed by 67R50. Remarkably, 76R0 exhibited the lowest N_f value, contrary to expectations for fatigue crack resistance. This observation is attributable to the blended RAP material that caused increased embrittlement in the HMA, leading to higher initial strength and resistance to cracking. However, increased embrittlement of the HMA compromises its potential to absorb fracture energy, resulting in a faster rate of crack propagation; see Table 7.

The Paris Law parameter, *n,* was found to correlate well with the anticipated fatigue cracking resistance; a higher *n* value indicated a more brittle AC material. It was found that the coefficient *n*, representing the slope of the fitted line, has a more significant impact on the overall model than the intercept, *Log(A)*. In this study, the coefficient *Log(A)* as the interception of fitting line is observed dominated by the coefficient *n* as the slope. Due to a substantial difference in *n* values, the *Log(A)* values are significantly influenced by the slope when extrapolated to a stress intensity factor of 1 (i.e., equivalent to 0 on a log scale). If asphalt mixtures have similar *n* values, *Log(A)* could be used to evaluate their relative cracking resistance. Additionally, the Paris' Law coefficients were observed to show relatively low CoV values compared to N_f. The CoV of Paris' law coefficient *n* varied from 12.7 to 16.7, and from 7.2 to 9.1 for the Paris' Law coefficient *Log(A);* see Table 7.

Table 7. Comparison results of sensitivity analysis mixtures

Mixture	J_c, kJ/m^2	Average			CoV		
		N_f	*n*	*Log(A)*	N_f	*n*	*Log(A)*
76R0	0.98	20952	3.275	-13.145	12.1	12.7	7.2
70R30	0.49	39464	4.009	-15.138	29.1	13.6	7.5
67R50	0.24	26798	4.847	-17.784	30.5	16.7	9.1

Figure 31 presents the relationships between the Paris' Law coefficients and J_c values. Strong linear correlations were observed between each Paris' Law coefficient and J_c, validating the use of these coefficients to distinguish mixtures based on their cracking resistance. However, further research is recommended to incorporate more mixtures with varying J_c (i.e., crack resistance) values to build a robust relationship between J_c and the Paris' Law coefficients.

Figure 31. Relationship between Paris' Law coefficients and critical strain release rate J_c

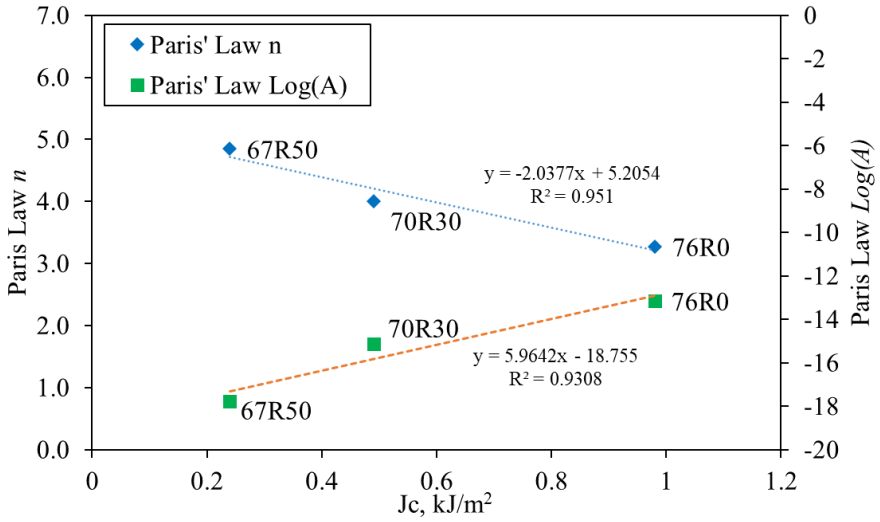

Figure 32 shows a graphical representation of the Paris' Law equation applied to the average coefficient values of the three mixtures. The solid lines indicate the stress intensity range covered in cyclic SCB tests, while dashed lines depict the extrapolated trends. Since different loading amplitudes were used for each mixture, the tested range of stress intensity factor was different.

At a specific low stress intensity factor value (i.e. $Log(K) = 2.0$), the ranking of crack growth rate was 67R50 < 70R30 < 76R0. Counterintuitively, this indicates a contradictory ranking of cracking resistance, as the "poor" mixture (67R50) exhibited the lowest cracking growth rate under these conditions. This discrepancy is attributable to the fact that mixture 67R50 showed the highest SCB strength due to its 50% RAP content. As the stress intensity factor increased, mixture 67R50 exhibited the fastest crack growth rate due to its highest *n,* which represents the slope of the Paris' Law equation. At higher stress intensity factor levels (i.e. $Log(K) = 3.1$), the ranking of crack growth rate becomes 76R0 < 70R30 < 67R50, which is consistent with the expected rank of cracking resistance. Given that the plotted crack growth rates are on a logarithmic scale and considering that crack growth rate is inherently the first derivative of crack length, it can be concluded that the cracking resistance of mixtures can be primarily determined using crack growth rate characteristics at higher stress intensity factor levels. This observation is consistent with established knowledge in the field.

Lower stress intensity factor values correspond to asphalt pavements in good condition. As the crack propagates within the asphalt pavement, tensile stresses become increasingly concentrated at the crack tip, which corresponds to the higher levels of stress intensity factor values. Although the mixtures with RAP material (70R30, 67R50) showed lower crack growth rates at a low stress intensity factor value, their higher Paris' Law *n* values suggest increased susceptibility to cracking over the long-term service life of the pavement.

Further, Figure 32 suggests that the range of the stress intensity factor is critical for accurately assessing cracking resistance through fracture tests. Although materials with high fracture strength, such as RAP blended HMA, exhibited a lower crack propagation rate at a low level of stress intensity factor, they may be highly susceptible to cracking at higher stress intensity factors, which corresponds to the long-term performance of asphalt pavement.

Figure 32. Paris' Law illustration on averaged coefficients for different mixtures

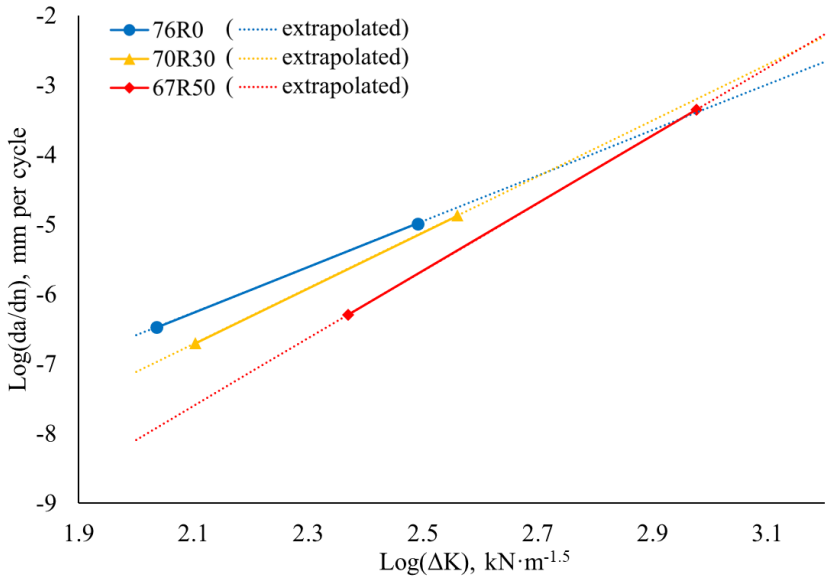

Results of the Developed Innovative Method

Statistical Analysis of Confidence Margins

Figures 33 to 35 present the statistical analysis of confidence margins (i.e., *sigma* value) determined based on the developed approach for the three mixtures (76R0, 70R30, and 67R50). Table 8 summarizes the results of the statistical analysis: the fitted parameters, μ and λ, for the inverse Gaussian distribution, the MSE of fitting, and the calculated criterion $sigma_{0.01}$. Four replicates were evaluated for each mixture.

Under the test setup used in this study, the inverse Gaussian parameters, μ and λ, showed slight variations across different mixtures and samples, indicating that the statistical model for the inverse Gaussian distribution is robust. The mean squared error (MSE) is a measure of the fitting accuracy, with lower MSE values indicating higher accuracy. For the mixture 76R0, the MSE ranged from 16.2 to 27.2, indicating good measurement accuracy. Mixture 70R30 exhibited even lower MSE values, ranging from 7.2 to 16.7, suggesting higher accuracy for this mixture. Mixture 67R50, however, showed a wider range of MSE values from 19.3 to 67.8, potentially due to higher aggregate anisotropy from mixtures with high RAP blending. Overall, the MSE values were relatively small compared to the squared PDF range (i.e., over 40,000), which suggests that the inverse Gaussian model fits well with the *sigma* distribution.

The f $sigma_{0.01}$ values demonstrated stability across different mixtures and samples, varying from 0.010 to 0.016. This observation indicates that under the same DIC setup and speckle manufacturing methods, the cracking criterion, $sigma_{0.01}$, determined from the developed approach is robust and reliable for the purpose of crack length identification.

Figure 33. Statistical analysis of *sigma*—Mixture 76R0

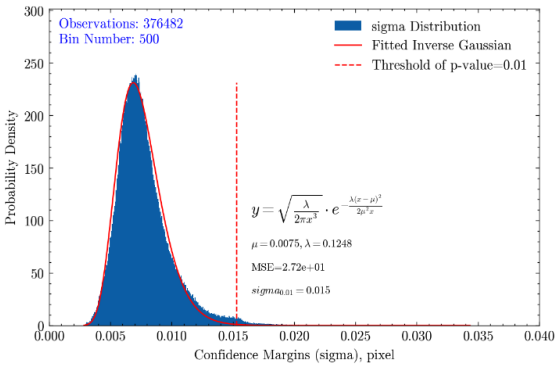

(a) Sample #1

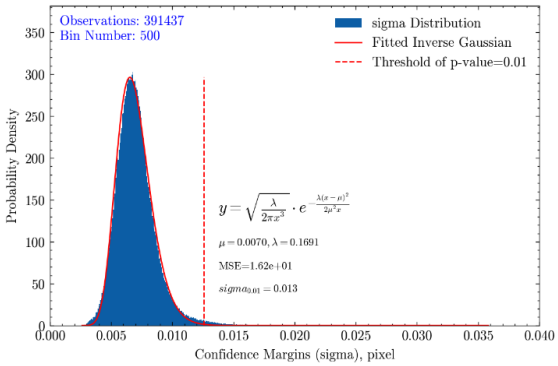

(b) Sample #2

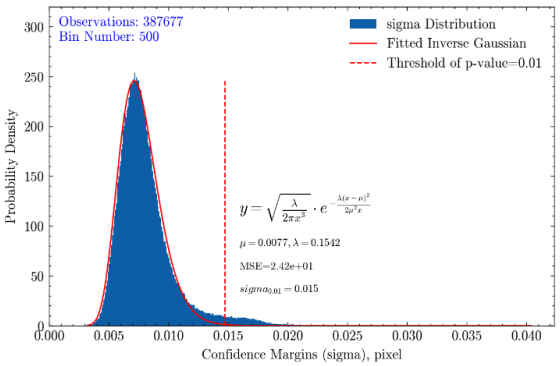

(c) Sample #3

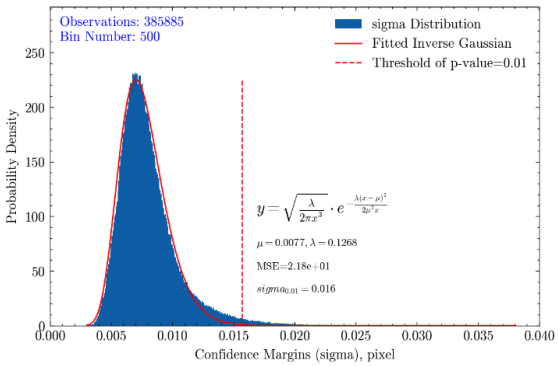

(d) Sample #4

Figure 34. Statistical analysis of *sigma*—Mixture 70R30

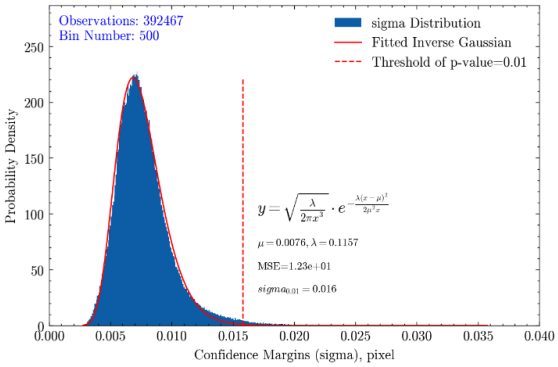

(a) Sample #1

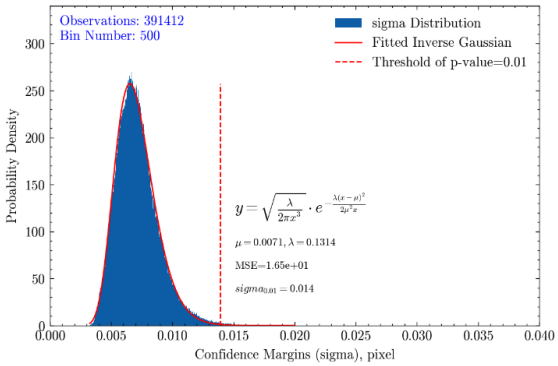

(b) Sample #2

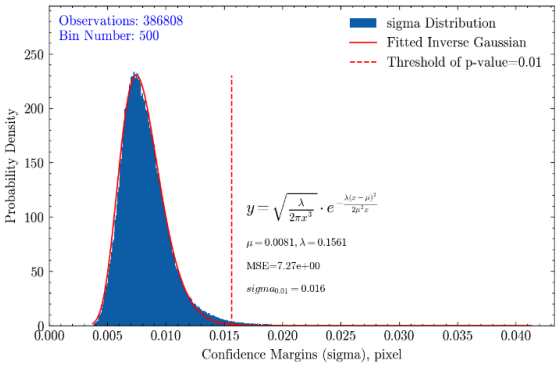

(c) Sample #3

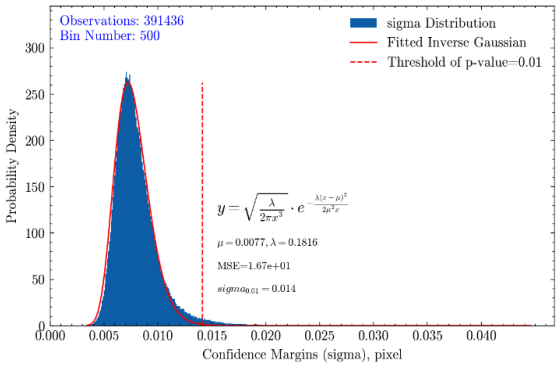

(d) Sample #4

Figure 35. Statistical analysis of *sigma*—Mixture 67R50

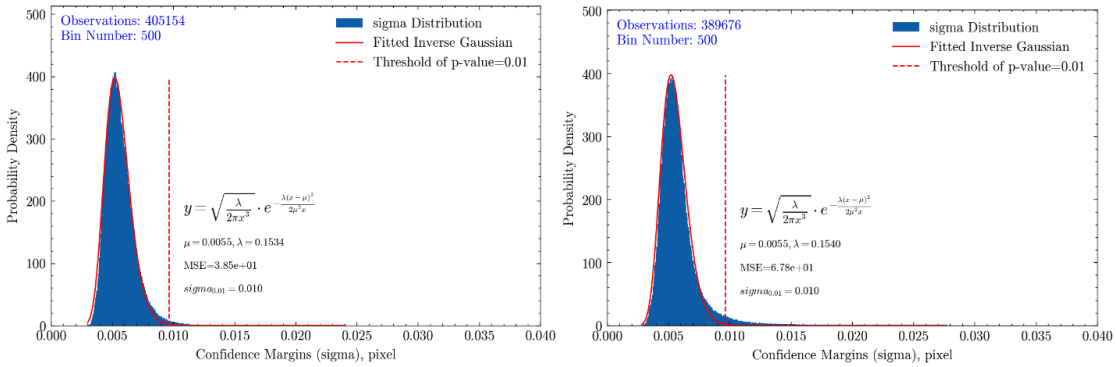

(a) Sample #1 **(b) Sample #2**

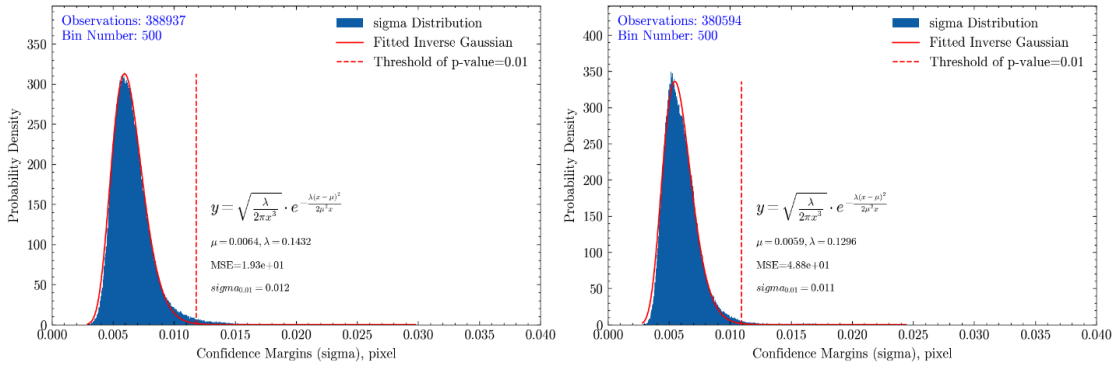

(c) Sample #3 **(d) Sample #4**

Table 8. Summary of statistical analysis results of confidence margins

Mixture	Sample	Inverse Gaussian - μ	Inverse Gaussian- λ	MSE	$Sigma_{0.01}$
76R0	Sample #1	0.0077	0.1542	24.2	0.015
	Sample #2	0.0070	0.1691	16.2	0.013
	Sample #3	0.0075	0.1248	27.2	0.015
	Sample #4	0.0077	0.1268	21.8	0.016
70R30	Sample #1	0.0081	0.1561	7.2	0.016
	Sample #2	0.0071	0.1314	16.5	0.014
	Sample #3	0.0076	0.1157	12.3	0.016
	Sample #4	0.0077	0.1816	16.7	0.014
67R50	Sample #1	0.0064	0.1432	19.3	0.012
	Sample #2	0.0055	0.1540	67.8	0.010
	Sample #3	0.0055	0.1534	38.5	0.010
	Sample #4	0.0059	0.1296	48.8	0.011

Paris' Law Coefficients Based on Confidence Margins

Table 9 shows a summary of the Paris' Law coefficients determined from the developed approach. The results were also compared with those determined from the previous approach, which was based on visual inspection and CMOD fitting to assess effectiveness and consistency; see Figures 36 and 37.

The Paris' Law results indicated that the developed *sigma*-based approach is effective in distinguishing between asphalt mixtures with varying fatigue cracking resistance. The measured Paris' Law coefficient values, *n,* from the developed approach for mixtures 76R0, 70R30, and 67R50 were 3.180, 4.387, and 5.678, respectively. Similar to the results determined from the previous CMOD-based approach, the Paris' Law *n* values showed a good correlation with the anticipated cracking resistance ranking of mixtures (76R0 > 70R30 > 67R50), where higher *n* values indicate a more brittle asphalt mixture.

To assess the consistency between the two approaches, t-tests were performed on Paris' Law *n* and *Log(A)* values, respectively. A significant level (i.e., alpha value) of 1% was used. The grouping results from the t-test are indicated as boxed letters within the figures. As the results

from the t-test indicated, the Paris' Law results from the developed *sigma*-based approach are consistent with those from the previous CMOD-based method. The innovative approach consistently yielded slightly higher average Paris' Law *n* values compared to the CMOD-based method across mixtures 76R0, 70R30, and 67R50. For instance, mixture 67R50 showed an average *n* value of 5.678 using the innovative approach versus 4.847 using the CMOD-based method. Additionally, the variation of Paris' Law coefficients determined from the developed approach between three mixtures suggests a potentially enhanced ability to differentiate mixtures in terms of fatigue crack resistance.

Table 9. Results of Paris' Law coefficients based on confidence margins

Mixture	Sample	Paris' Law Results	
		n	***Log(A)***
76R0	Sample #1	2.653	-11.716
	Sample #2	3.476	-13.810
	Sample #3	3.554	-13.560
	Sample #4	3.038	-12.689
70R30	Sample #1	4.474	-15.653
	Sample #2	3.407	-13.466
	Sample #3	5.088	-17.689
	Sample #4	4.578	-16.430
67R50	Sample #1	6.466	-21.645
	Sample #2	6.661	-23.184
	Sample #3	5.098	-19.185
	Sample #4	4.485	-16.803

Figure 36. Comparison results of Paris' Law coefficient *n*

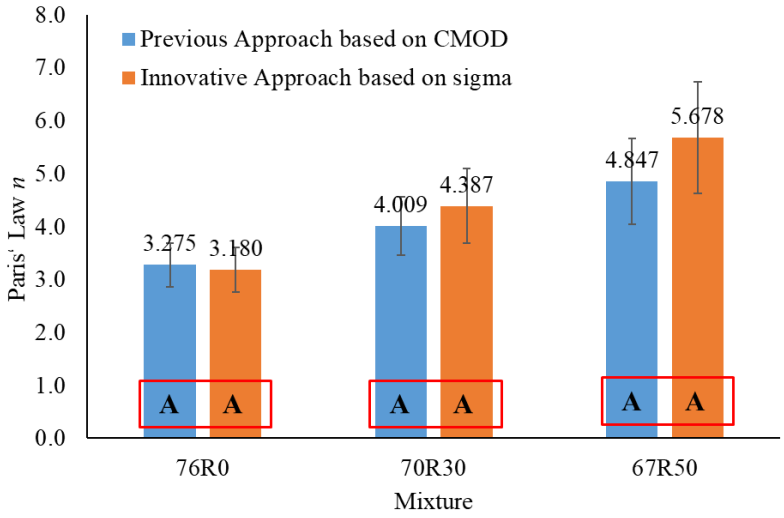

Figure 37. Comparison results of Paris' Law coefficient *Log(A)*

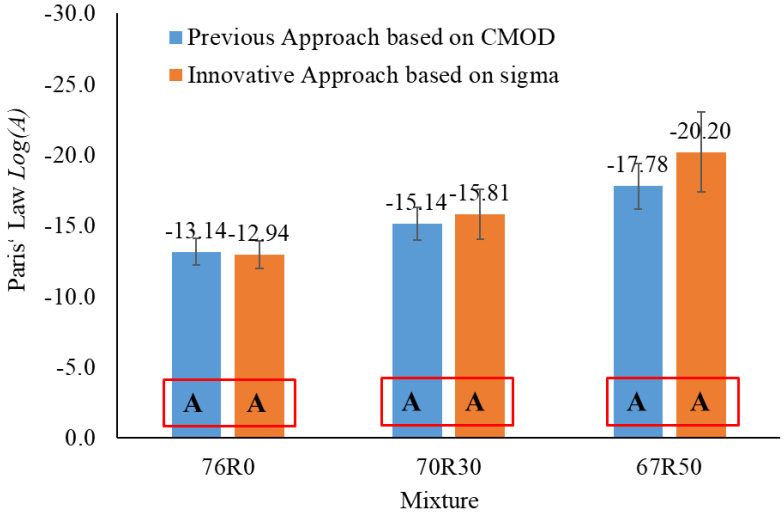

Prediction Results of Pavement Fatigue Life

Dynamic Modulus Test Results

The dynamic modulus master curves were constructed using the time-temperature superposition principle. In this study, a reference temperature of 21.1°C was used. Figure 38 presents the dynamic modulus master curves for the three sensitivity analysis mixtures. It is noted that the 67R50 mixture incorporating 50% RAP exhibited the highest stiffness, and the 70R30 mixture incorporating 30RAP was stiffer than the 76R0 mixture, which contained no RAP.

Figure 38. Dynamic modulus results for sensitivity analysis mixtures

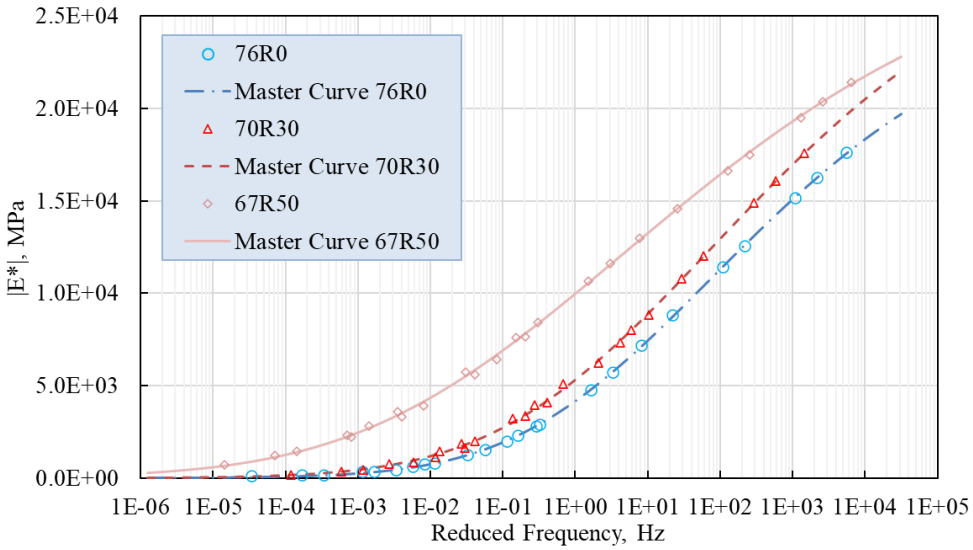

Pavement Mechanic Response Results

The pavement's mechanical responses, including tensile strain and tensile stress, were computed from the FE simulation. In the FE model, the asphalt mixture was treated as a linear viscoelastic continuum, where the dynamic modulus data was used as inputs for AC material properties. Figure 39 and Figure 40 show the tensile strain and tensile stress values for pavement mechanistic responses, respectively.

Figure 39. Pavement mechanistic response results—tensile strain

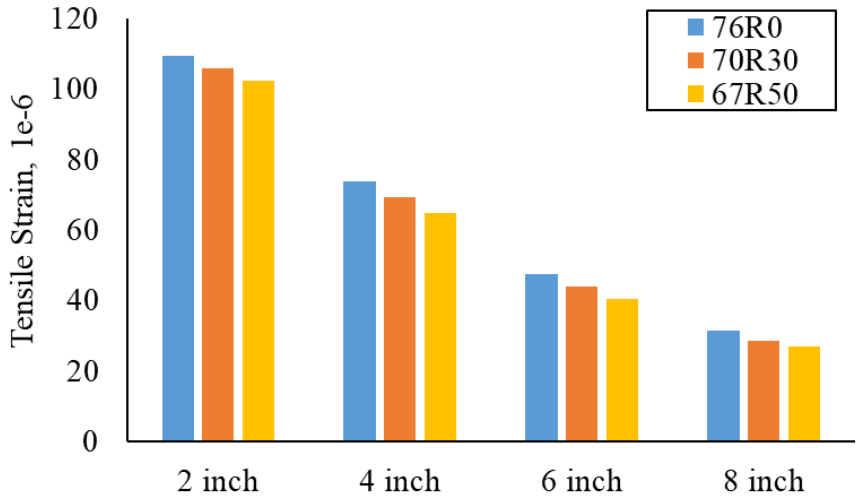

Figure 40. Pavement mechanistic response results—tensile stress

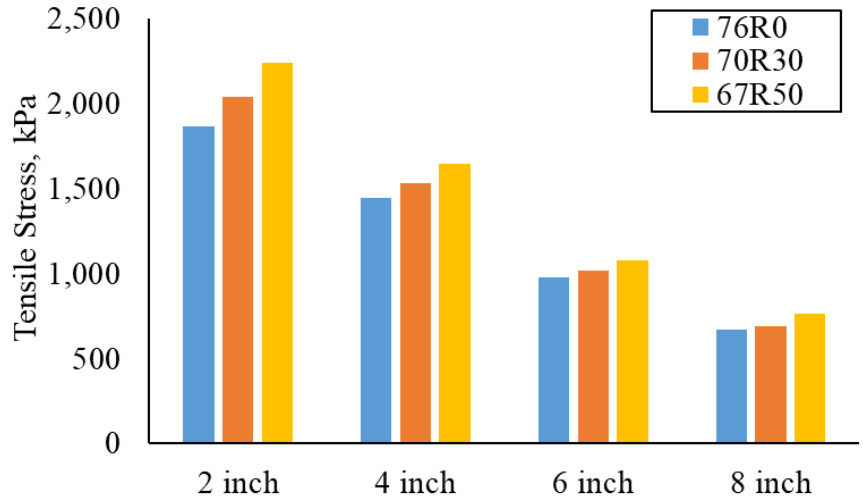

Prediction Results of Pavement Fatigue Model Based on Paris' Law Equation

Figure 41 and Figure 42 present the fatigue life results for the Pavement ME model and Paris' Law-based fatigue model, respectively. It is noted that a direct comparison between these two models may not be applicable due to their distinct methodologies. While the Paris' Law model is based on fracture mechanics principles and lacks validation using field data, the Pavement ME model primarily relies on empirical approaches and calibrates its coefficients using extensive field data. Both the Pavement ME fatigue model and Paris' Law-

based model were shown to be effective in predicting the fatigue life of the asphalt mixtures. The predicted fatigue lives were consistent with the anticipated ranking of fatigue cracking performance of the mixtures.

However, the Paris' Law-based model demonstrated greater sensitivity to the mixtures with varying cracking performances. Using the Pavement ME fatigue model, the predicted fatigue life for the mixture 76R0 of 6-in. asphalt layer is approximately 10% longer than that of the mixture 67R50 of 6-in. asphalt layer. In contrast, the Paris' Law-based model predicted a fatigue life for the 76R0 mixture of 6-in. asphalt layer that was more than ten times longer than that for the 67R50 mixture of 6-in. asphalt layer, suggesting a higher sensitivity to mixture cracking performance differences. These findings underscore the importance of considering the underlying principles when selecting and interpreting fatigue models for asphalt pavement analysis, emphasizing the need for further investigation into fracture mechanics-based methods for the characterization of asphalt mixture fatigue cracking.

Figure 41. Fatigue life prediction results of Pavement ME model

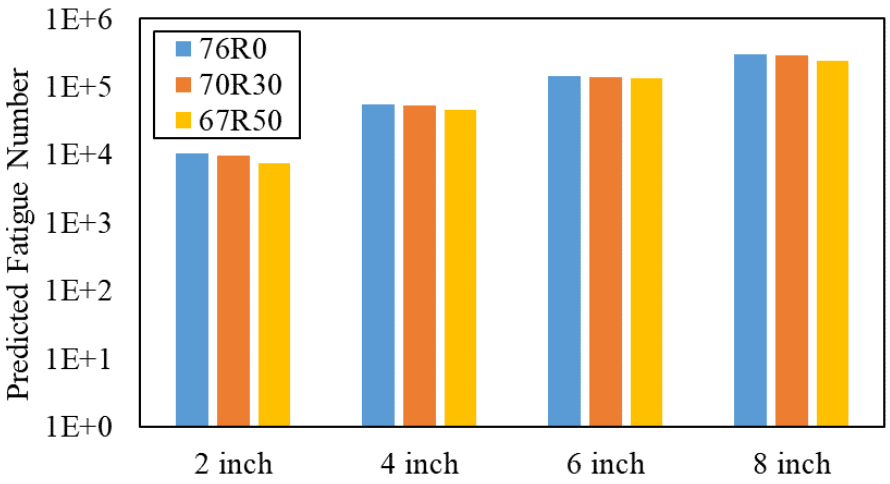

Figure 42. Fatigue life prediction results of Paris' Law-based model

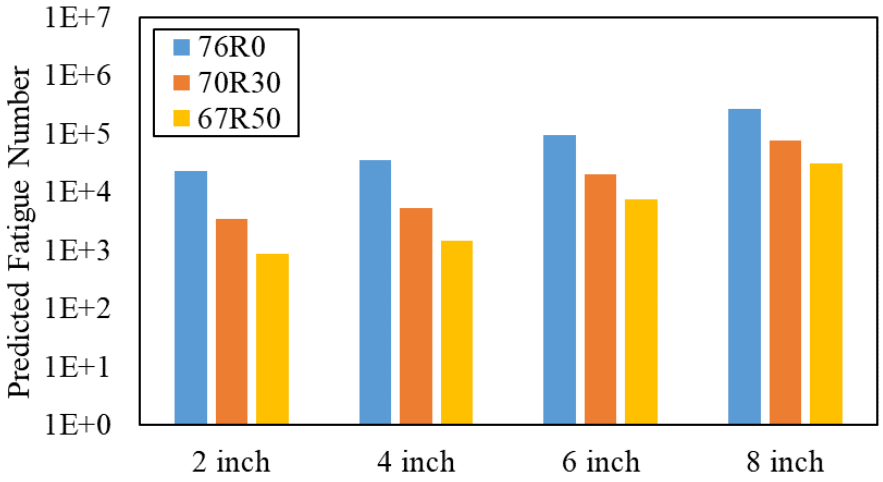

Preliminary Calibration of Modified Pavement ME Model

Table 10 presents the results of Paris' Law coefficients and the fatigue life N_f measured from ALF test for the mixtures L8 and L11. Additionally, the critical strain energy release rate J_c measured from the monotonic SCB test were presented, which is sourced from previous study [52]. The mixture L11 exhibited superior cracking resistance compared to L8 in terms of fatigue life measured by ALF. The results of SCB-J_c and Paris' Law coefficients measured from cyclic SCB test also indicated that mixture L11 is of better cracking resistance.

Table 10. Laboratory and field performance results for ALF mixtures

Mixture	N_f (ALF)	SCB-J_c	Cyclic SCB Test	
			n	***Log(A)***
L8	47679	0.47	4.845	-18.353
L11	81044	0.59	3.353	-14.676

The capacity of the modified Pavement ME model was evaluated, and the prediction results of pavement fatigue life were compared to the original Pavement ME model. The model input of tensile strain responses for the ALF mixtures were obtained from previous study [52]. The coefficients C_2, β_{f4}, and β_{f5} of the modified Pavement ME Model are preliminarily calibrated by the two data points of ALF mixtures. Figure 43 presents the calibration results. First, the coefficients of β_{f4} and β_{f5} were assumed to be "1" and the coefficient C_2 is calibrated by mixture L8. It is observed that the rank of fatigue life predicted by the modified

Pavement ME model is consistent with the measured ones, whereas the fatigue life predicted by the original Pavement ME is not.

Figure 43. Calibration of the modified Pavement ME model

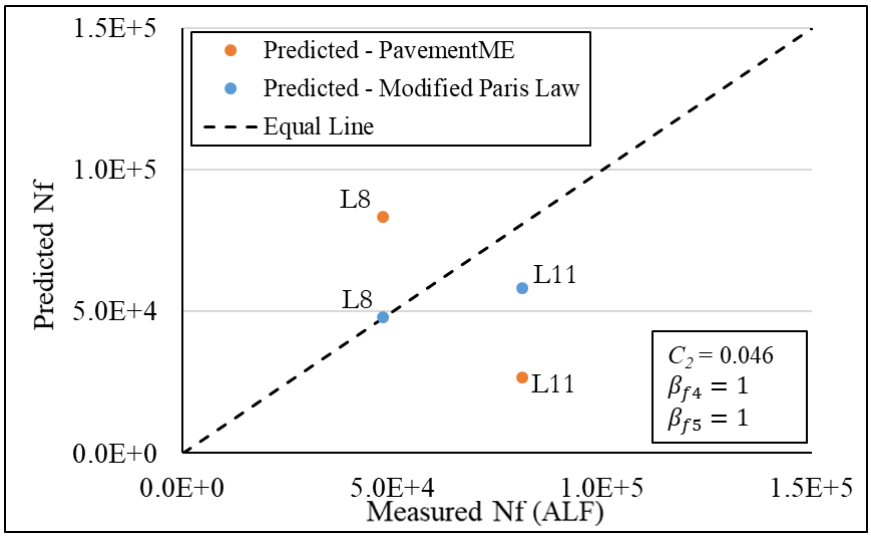

(a) Assumed β_{f4} and β_{f5} be "1"

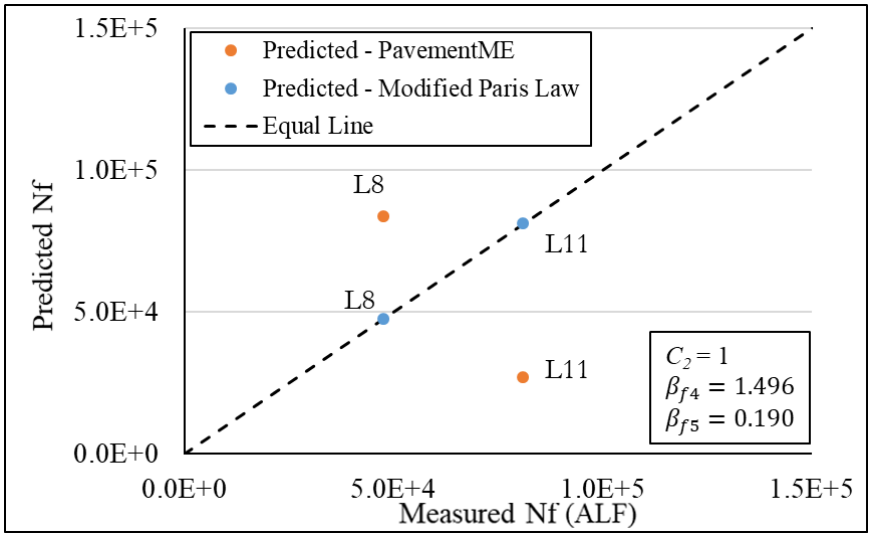

(b) Calibrated by the measured N_f

Next, the coefficients β_{f4}, and β_{f5} were calibrated by both data points of mixtures L8 and L11, while the coefficient C_2 remained at "1." The predicted N_f was perfectly matched to the measured N_f due to limited data points of "2" in this study. However, the modified Pavement ME model provided a way for the improved prediction of pavement fatigue life. The

calibration of the developed model can be extended by incorporating additional mixtures evaluated through laboratory tests and field performance data.

Conclusions

The primary objective of this project was to develop a cyclic SCB test to characterize the fatigue cracking properties of asphalt mixtures at intermediate temperatures. A secondary goal was to apply the Paris' Law coefficients obtained from the proposed cyclic SCB test in the pavement fatigue model to predict pavement fatigue life.

To fulfill the objectives of the study, the DIC system was employed for the monitoring and measurement of crack propagation during the cyclic SCB test. The DIC system configurations were set up for deformation and crack propagation measurements of test specimens during cyclic SCB testing. Four asphalt mixtures were identified and selected for the experimental program. Crack length measurements obtained during the cyclic SCB test were used to fit the Paris' Law equation. Three indicators measured from the cyclic SCB test were used to characterize the fatigue cracking properties of the asphalt mixtures evaluated: the number of cycles to failure N_f, and the Paris' Law coefficients, n and $Log(A)$. Optimized testing parameters were selected based on the variability of the cracking performance indicator values and practical considerations. A sensitivity analysis was performed for the proposed cyclic SCB test protocol using three asphalt mixtures with varying cracking resistance. An innovative method was developed to directly measure the crack length during the cyclic SCB test. Additionally, the Paris' Law coefficient values derived from the cyclic SCB test were utilized to predict the fatigue life of asphalt pavements. Based on the findings of the study, the following conclusions were drawn:

- The variance of the results obtained from the cyclic SCB test showed that it is repeatable. Based on test variability and practicality, a notch depth of 25 mm and a loading frequency of 10 Hz were recommended as optimal parameters for the cyclic SCB test at intermediate temperatures.
- The Paris' Law coefficients obtained from the cyclic SCB tests showed relatively lower variance values than N_f. Based on statistical analysis, N_f was found to be dependent on the notch depth and loading frequency parameters of the cyclic SCB test. N_f increased with decreasing notch depth and increasing loading frequency, whereas the Paris' Law coefficients are independent of notch depth or loading frequency, suggesting that the Paris' Law coefficients represent fundamental material properties.
- The Paris' Law coefficient n exhibited a strong correlation with the anticipated ranking of fatigue cracking resistance of the mixtures considered.

- The range of stress intensity factor values is critical to evaluate the cracking resistance of asphalt mixtures through fracture testing. Although materials with high fracture strength, such as RAP blended HMA, exhibit lower crack propagation rates at low stress intensity factor values, they may be highly susceptible at higher stress intensity factor values, which correspond with the long-term performance of asphalt pavements.
- The innovative approach developed in this study utilized DIC confidence margins (i.e., *sigma*) to directly and efficiently identify and measure the crack length during the cyclic SCB test, which overcame the limitations of previous approaches that relied on indirect estimation and manual labeling during the analysis process.
- Compared to the mechanistic-empirical Pavement ME fatigue model, the fracture mechanics-based Paris' Law model showed greater sensitivity to variations in mixture cracking performance.
- A modified Pavement ME model is developed for predicting pavement fatigue life by introducing inputs of the Paris' Law coefficients measured by the developed cyclic SCB test. The improved prediction results were observed from the modified Pavement ME model compared to the original Pavement ME model.

Recommendations

This study developed and validated a cyclic SCB test protocol coupled with Digital Image Correlation (DIC) for the evaluation of the fatigue cracking performance of asphalt mixtures. The following is recommended:

- Characterize pavement cores using the developed cyclic SCB test to further validate the test protocol with field performance.
- Adopt modified Pavement ME fatigue model based on fracture mechanics principles and Paris' Law indicators.
- Develop correlation analysis amongst monotonic SCB J_c, cyclic SCB n and $Log(A)$, and field performance.
- Initiate a research project to catalog Paris' Law indicators (n, $Log(A)$) for Louisiana mixtures for potential assessment of asphalt mixtures' fatigue life perdition.

Acronyms, Abbreviations, and Symbols

Term	Description
AASHTO	American Association of State Highway and Transportation Officials
AC	Asphalt Concrete
ALF	Accelerated Loading Facility
AMPT	Asphalt Mixture Performance Tester
ANOVA	Analysis of Variance
ASTM	American Society of Testing Materials
cm	centimeter(s)
CCA	Connected Component Analysis
COMD	Crack Opening Mouth Displacement
CoV	Coefficient of Variation
DIC	Digital Image Correlation
DOTD	Louisiana Department of Transportation and Development
FE	Finite Element
FHWA	Federal Highway Administration
ft.	foot (feet)
in.	inch(es)
LA	Louisiana
LTRC	Louisiana Transportation Research Center
LVDT	Linear Variable Differential Transducer
lb.	pound(s)
ME	Mechanistic-Empirical
m	meter(s)
MTS	Material Testing System
NMAS	Nominal Maximum Aggregate Size
RBR	Recycled Binder Ratio
WMA	Warm Mix Asphalt

References

[1] American Society for Testing Materials, "Standard test method for evaluation of asphalt mixture cracking resistance using the Semi-Circular Bend (SCB) test at intermediate temperatures," *ASTM D8044-23, ASTM International,* West Conshohocken, PA, 2023.

[2] E. Mahmoud, S. Saadeh, H. Hakimelahi and J. Harvey, "Extended finite-element modeling of asphalt mixtures' fracture properties using the Semi-Circular Bend test," *Road Materials and Pavement Design,* vol. 15, pp. 153-166, 2014.

[3] S. B. Cooper Jr., L. N. Mohammad and M. A. Elseifi, "Laboratory performance of asphalt mixtures containing recycled asphalt shingles," *Transportation Research Record,* vol. 2445, pp. 94-102, 2014.

[4] L. N. Mohammad, M. Kim and H. Challa, "Development of performance-based specifications for Louisiana asphalt mixtures," 2016.

[5] L. N. Mohammad, M. Kim and M. A. Elseifi, "Characterization of asphalt mixtures' fracture resistance using the Semi-Circular Bend test," in *7th RILEM International Conference on Cracking in Pavements: Mechanisms, Modeling, Testing, Detection and Prevention Case Histories*.

[6] S. B. Cooper III, L. N. Mohammad, S. Kabir and W. King Jr, "Balanced asphalt mixture design through specification modification: Louisiana's experience," *Transportation Research Record,* vol. 2447, pp. 92-100, 2014.

[7] P. Paris and F. Erdogan, "A critical analysis of crack propagation laws," 1963.

[8] B. Huang, X. Shu and G. Zuo, "Using notched Semi-Circular Bend fatigue test to characterize fracture resistance of asphalt mixtures," *Engineering Fracture Mechanics,* vol. 109, pp. 78-88, 2013.

[9] L. Cheng, L. Zhang, X. Liu, F. Yuan, Y. Ma and Y. Sun, "Evaluation of the fatigue properties for the long-term service asphalt pavement using the Semi-Circular Bend tests and stereo digital image correlation technique," *Construction and Building Materials,* vol. 317, p. 126119, 2022.

[10] T. C. Chu, W. F. Ranson and M. A. Sutton, "Applications of digital-image-correlation techniques to experimental mechanics," *Experimental Mechanics,* vol. 25, pp. 232-244, 1985.

[11] B. Birgisson, A. Montepara, E. Romeo, R. Roncella, R. Roque and G. Tebaldi, "An optical strain measurement system for asphalt mixtures," *Materials and Structures,* vol. 42, pp. 427-441, 2009.

[12] G. R. Chehab, Y. Seo and Y. R. Kim, "Viscoelastoplastic damage characterization of asphalt-aggregate mixtures using digital image correlation," *International Journal of Geomechanics,* vol. 7, pp. 111-118, 2007.

[13] I. L. Al-Qadi, I. M. Said, U. M. Ali and J. R. Kaddo, "Cracking prediction of asphalt concrete using fracture and strength tests," *International Journal of Pavement Engineering,* vol. 23, pp. 3333-3345, 2022.

[14] J. Zhang, M. Sakhaeifar, D. N. Little, A. Bhasin and Y. R. Kim, "Characterization of crack growth rate of sulfur-extended asphalt mixtures using cyclic Semi-Circular Bend test," *Journal of Materials in Civil Engineering,* vol. 30, p. 04018311, 2018.

[15] F. T. S. Aragão and Y. R. Kim, "Mode I fracture characterization of bituminous paving mixtures at intermediate service temperatures," *Experimental Mechanics,* vol. 52, pp. 1423-1434, 2012.

[16] B. Hill and W. G. Buttlar, "Evaluation of polymer modification in asphalt mixtures through digital image correlation and performance space diagrams," *Construction and Building Materials,* vol. 122, pp. 667-673, 2016.

[17] C. Xing, Y. Tan, X. Liu, K. Anupam and T. Scarpas, "Research on local deformation property of asphalt mixtures using digital image correlation," *Construction and Building Materials,* vol. 140, pp. 416-423, 2017.

[18] K. P. Chong and M. D. Kuruppu, "New specimen for fracture toughness determination for rock and other materials," *International Journal of Fracture,* vol. 26, pp. R59-R62, 1984.

[19] R. L. Krans, F. Tolman and M. F. Van De Ven, "Semi-Circular Bend test: a practical crack growth test using asphalt concrete cores," in *International RILEM Conference on Reflective Cracking in Pavements, 3rd, 1996, Maastricht, The Netherlands*.

[20] M. A. Mull, A. Othman and L. Mohammad, "Fatigue crack propagation analysis of chemically modified crumb rubber-asphalt mixtures," *Journal of Elastomers & Plastics,* vol. 37, pp. 73-87, 2005.

[21] Z. Wu, L. N. Mohammad, L. B. Wang and M. A. Mull, "Fracture resistance characterization of superpave mixtures using the Semi-Circular Bend test," ASTM International, 2005.

[22] X. Shu, B. Huang and D. Vukosavljevic, "Evaluation of cracking resistance of recycled asphalt mixture using Semi-Circular Bend test," in *Paving Materials and Pavement Analysis*, 2010, pp. 58-65.

[23] S. Im, Y. R. Kim and H. Ban, "Rate-and temperature-dependent fracture characteristics of asphaltic paving mixtures," *Journal of Testing and Evaluation,* vol. 41, pp. 257-268, 2013.

[24] R. Hofman, B. Oosterbaan, S. M. J. G. Erkens and J. van der Kooij, "Semi-Circular Bend test to assess the resistance against crack growth," in *6th RILEM Symposium on Performance Testing and Evaluation of Bituminous Materials*.

[25] M. M. Hassan and H. A. Khalid, "Fracture characteristics of asphalt mixtures containing incinerator bottom ash aggregate," *Transportation Research Record,* vol. 2180, pp. 1-8, 2010.

[26] I. L. Lim, I. W. Johnston and S. K. Choi, "Stress intensity factors for semi-circular specimens under three-point bending," *Engineering Fracture Mechanics,* vol. 44, pp. 363-382, 1993.

[27] R. A. Schapery, "A theory of crack initiation and growth in viscoelastic media: I. Theoretical development," *International Journal of Fracture,* vol. 11, pp. 141-159, 1975.

[28] R. C. Van Rooijen and A. H. De Bondt, "Crack propagation performance evaluation of asphaltic mixes using a new procedure based on cyclic Semi-Circular Bend tests," *Pavement Cracking: Mechanisms, Modeling, Detection, Testing, and Case Histories,* pp. 437-446, 2008.

[29] J. Jiang, F. Ni, F. Wu, H. Sadek and Q. Lv, "Evaluation of the healing potential of asphalt mixtures based on a modified Semi-Circular Bend test," *Construction and Building Materials,* vol. 196, pp. 284-294, 2019.

[30] F. Yuan, L. Cheng, X. Shao, Z. Dong, L. Zhang, G. Wu and X. He, "Full-field measurement and fracture and fatigue characterizations of asphalt concrete based on the SCB test and stereo-DIC," *Engineering Fracture Mechanics,* vol. 235, p. 107127, 2020.

[31] H. Jiang-san, W. Lan and L. Xin, "Anti-fatigue performance of warm-mixed rubber powder modified asphalt mixture based on the DIC technique," *Construction and Building Materials,* vol. 335, p. 127489, 2022.

[32] J. M. Hutt and A. E. Salam, "Dynamic stability of plates by finite elements," *Journal of the Engineering Mechanics Division,* vol. 97, pp. 879-899, 1971.

[33] K. Majidzadeh, E. M. Kauffmann and D. V. Ramsamooj, "Application of fracture mechanics in the analysis of pavement fatigue," in *Association of Asphalt Paving Technologists Proc*.

[34] C. L. Monismith and Y. M. Salam, "Distress characteristics of asphalt concrete mixes," in *Association of Asphalt Paving Technologists Proc*.

[35] T. L. Anderson, "Fracture Mechanics: Fundamentals and Applications," CRC Press, 2017.

[36] C. Solutions, Vic-3D Manual, Columbia, SC: Correlated Solutions. Inc., 2010.

[37] M. A. Sutton, J. J. Orteu and H. Schreier, "Image Correlation for Shape, Motion, and Deformation Measurements: Basic Concepts, Theory, and Applications," Springer Science & Business Media, 2009.

[38] G. Saha and K. P. Biligiri, "Comprehensive fatigue mechanism of asphalt mixtures: Synergistic study of crack initiation and propagation," *Journal of Materials in Civil Engineering,* vol. 30, p. 04018024, 2018.

[39] Louisiana Department of Transportation and Development, Louisiana Standard Specifications for Roads and Bridges: 2016 Edition, Louisiana Department of Transportation and Development, 2016.

[40] American Association of State Highway and Transportation Officials, Standard Practice for Mixture Conditioning of Hot Mix Asphalt, vol. R 30, United States: American Association of State Highway and Transportation Officials, 2002.

[41] B. D. Lucas and T. Kanade, "An iterative image registration technique with an application to stereo vision," in *IJCAI'81: 7th International Joint Conference on Artificial Intelligence*.

[42] M. J. Schervish and M. H. DeGroot, "Probability and Statistics," vol. 563, Pearson Education London, UK: 2014.

[43] K. Wu, E. Otoo and K. Suzuki, "Optimizing two-pass connected-component labeling algorithms," *Pattern Analysis and Applications,* vol. 12, p. 117-135, 2009.

[44] American Association of State Highway and Transportation Officials, Standard Method of Test for Determining Dynamic Modulus of Hot Mix Asphalt (HMA), vol. AASHTO TP 62, Washington DC: AASHTO, 2010.

[45] American Association of State Highway and Transportation Officials, *AASHTOWare Pavement ME Design.*

[46] Y. R. Kim, M. N. Guddati, Y. T. Choi, D. Kim, A. Norouzi, Y. D. Wang, B. Keshavarzi, M. Ashouri, A. Ghanbari and A. Wargo, "Hot-mix asphalt performance related specification based on viscoelastoplastic continuum damage (VEPCD) models," 2022.

[47] Y. Wang, A. Norouzi and Y. R. Kim, "Comparison of fatigue cracking performance of asphalt pavements predicted by pavement ME and LVECD programs," *Transportation Research Record,* vol. 2590, pp. 44-55, 2016.

[48] N. Sudarsanan and Y. R. Kim, "A critical review of the fatigue life prediction of asphalt mixtures and pavements," *Journal of Traffic and Transportation Engineering (English Edition),* vol. 9, pp. 808-835, 2022.

[49] L. Mohammad, W. Cao and P. Barghabany, "Design and Analysis Procedures for Asphalt Mixtures Containing High RAP Contents and/or RAS," 2021.

[50] X. Li and N. Gibson, "Comparison of asphalt mixture performance tester fatigue characteristics with full scale pavement cracking for recycled and warm mix asphalts," *Transportation Research Record: Journal of the Transportation Research Board,* vol. 85, 2016.

[51] D. B. Duncan, "Multiple range and multiple F tests," *Biometrics,* vol. 11, pp. 1-42, 1955.

[52] W. Cao, L. N. Mohammad, M. A. Elseifi, S. B. Cooper, and S. Saadeh, "Fatigue performance prediction of asphalt pavement based on Semi-Circular Bend test at intermediate temperature," *Journal of Materials in Civil Engineering,* vol. 30, p. 04018219, 2018.

Appendix A

Finite Element Modeling and Mechanic Response of Asphalt Pavement

Pavement Structure

Three layers of asphalt concrete, unbound aggregate base, and subgrade were used for FE modeling. The structure thickness for each layer are listed in Table A-1.

Table A-1. Pavement structure for Finite Element modeling

Layer Type	Thickness, cm
Asphalt Concrete	10
Unbound Aggregate Base	20
Subgrade	380

Material Properties

The dynamic modulus data is converted to Prony Series as material properties inputs of AC layer, which is listed in Table A-2. The material properties of base and subgrade layers are listed in Table A-3.

Table A-2. Material properties for AC layer

Relaxation Time, sec.	Prony series coefficients, kPa		
	Mixture 76R0	Mixture 70R30	Mixture 67R50
Infinite	8.90E+02	9.10E+02	9.50E+02
1.00E+08	1.84E+02	1.85E+02	4.03E+05
1.00E+07	1.02E+04	1.30E+04	1.76E+05
1.00E+06	3.05E+04	5.33E+04	1.81E+05
1.00E+05	8.46E+04	1.86E+05	1.03E+06
1.00E+04	2.61E+05	4.14E+05	1.56E+06
1.00E+03	7.03E+05	1.08E+06	2.41E+06

Relaxation Time, sec.	Prony series coefficients, kPa		
	Mixture 76R0	Mixture 70R30	Mixture 67R50
1.00E+02	1.73E+06	2.08E+06	3.04E+06
1.00E+01	2.90E+06	3.18E+06	3.36E+06
1.00E+00	3.70E+06	3.96E+06	3.32E+06
1.00E-01	4.09E+06	4.37E+06	3.11E+06
1.00E-02	3.57E+06	3.77E+06	2.63E+06
1.00E-03	2.97E+06	2.98E+06	2.06E+06
1.00E-04	5.71E+07	5.71E+07	5.25E+07
1.00E-05	3.29E+08	3.29E+08	3.29E+08
1.00E-06	8.31E+08	8.31E+08	8.31E+08
1.00E-07	2.07E+09	2.07E+09	2.02E+09

Table A-3. Material properties for base and subgrade layer

Layer Type	Elastic Modulus, kPa	Poisson's Ratio
Unbound Aggregate Base	2.07E+05	0.35
Subgrade	6.89E+04	0.40

Climate Data

For comparable analysis with AASHTO fatigue model, the temperature for full depth of pavement structures were set as isothermal 20℃.

Traffic Loading

For traffic loading, the standard single-axle dual tires load is employed. The tire pressure for each tire in this configuration is 827.37 kPa. The spacing between the dual tires is set at 30.47 cm. The velocity is set to 27 m/sec. to simulate a vehicle traveling at a speed of 80 km/hr.

Mechanic Response Results

The critical point of tensile stress and tensile strain is found as the center point of the bottom of AC layer. Figure A-1 shows the spatial distribution of tensile stress in pavement structure. Figures A-1 and A-2 shows the examples of temporal distribution of tensile stress and tensile strain at the critical point, respectively.

Figure A-1. Spatial distribution of tensile stress (S_{yy})

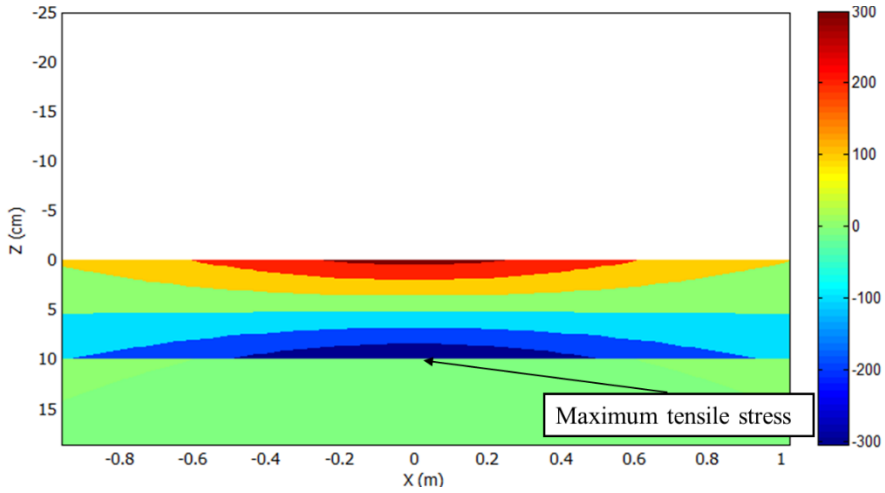

Figure A-2. Tensile stress at critical point of bottom of AC layer

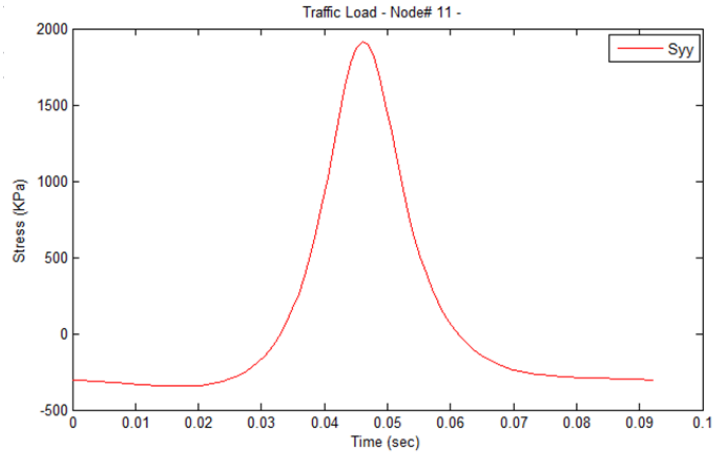

Figure A-3. Tensile stress at critical point of bottom of AC layer